Nanoscale

PAPER

Cite this: *Nanoscale*, 2020, **12**, 904

Nanoparticle-based photothermal heating to drive chemical reactions within a solid: using inhomogeneous polymer degradation to manipulate mechanical properties and segregate carbonaceous by-products†

Honglu Huang,[a] Gabriel Firestone,[b] Daniela Fontecha,[b] Russell E. Gorga,[a] Jason R. Bochinski *[b] and Laura I. Clarke *[b]

Photothermal heating *via* metal nanoparticles is utilized to degrade polyethylcyanoacrylate (PECA), which undergoes a thermally-driven depolymerization process, resulting in (i) monomer loss from the sample, (ii) repolymerization to form shorter chains (oligomer), and (iii) formation of carbonaceous by-products which are graphene-like and luminescent. These unique PECA properties are used to demonstrate the heterogeneous temperature distribution present during photothermal processing and the results are compared to degradation *via* conventional methods where a uniform temperature is present. Photothermal heating results in formation of pockets of depolymerized material around each nanoscale heating site. The characteristic size of these photothermally-generated mechanical defects is determined from changes in the material's tensile strength. Changes in mass loss and molecular weight are utilized to determine the fraction of the sample that has depolymerized: distributing this volume equally to each heating site (based on the nanoparticle concentration) results in a volume that matches the defect size from independent mechanical measurements. In this way, macroscopic measurements elucidate the mesoscopic pattern of photothermal degradation. Sample morphology on scales from millimeters to nanometers is assessed *via* optical and electron microscopy. The carbonaceous by-products of degradation form in the hot region around each nanoparticle during photothermal heating, as revealed by transmission electron microscopy studies. Heterogeneous heating is also evident from optical images where starch granules, employed as an inert dilute additive to enhance PECA mechanical properties, also become luminescent due to degradation in "hot spots" created by the overlap of warm regions from nearby nanoparticle sites. Beyond the fundamental knowledge gained by these studies, the results demonstrate the ability to manipulate the connection between mechanical properties and chemical degradation which is important for developing new strategies for management of polymeric waste.

Received 27th August 2019,
Accepted 30th November 2019

DOI: 10.1039/c9nr07401e

rsc.li/nanoscale

1. Introduction

The principles of green engineering[1] postulate that an object should remain fully useful for its desired lifetime, and then be controllably transformed into harmless by-products, however polymeric materials often present a challenge within this idealized framework. Decades of research[2–4] has focused on developing commercial polymers which overcome their innate propensity to deteriorate under normal use and discovering means to increase resiliency to elongate length of service and ensure highly reliable, robust mechanical properties. The resulting materials are typically long-lived and inexpensive, but can neither be indefinitely recycled nor efficiently degraded under typical landfill conditions.[5] Furthermore,

[a]*Fiber and Polymer Science Program, NC State University, Raleigh, NC 27695, USA*
[b]*Department of Physics, NC State University, Raleigh, NC 27695, USA.*
E-mail: jason_bochinski@ncsu.edu, laura_clarke@ncsu.edu

†Electronic supplementary information (ESI) available: Fig. S1: Characteristic stress–strain curves for as-made and highly-degraded PECA : starch composite samples. Fig. S2: Scanning electron microscopy images of sample surface before and after heat treatment. Fig. S3: Fluorescence microscopy images of the luminescence from starch granules after thermal treatment at high temperatures. Fig. S4: Schematic diagram of light intensity timing curve for the photothermal heating and temperature-measurement light sources. Fig. S5: Comparison of emission spectra from as-made PECA : starch and degraded PECA samples. See DOI: 10.1039/C9NR07401E

when plastic products escape outside of a waste management cycle (*i.e.*, become unconfined in the environment), the chemical degradation rate is slow and loss of mechanical stability occurs on moderate time scales.[1] Reduction of mechanical properties hinders re-collection and environmental cleanup as the waste objects fracture, potentially forming fragments which are largely un-degraded chemically. The resulting polymeric micro-shards can harbor and concentrate chemically-similar hydrophobic toxins (particularly in ocean and sea environments) and have a characteristic size that can readily enter the food cycle of a wide range of wildlife.[6]

Alternative degradation strategies that adjust the connection between mechanical failure and chemical decomposition represent a powerful tool to address management of polymeric objects at the end-of-service. For example, when bacterial remediation of a partially degraded polymer is intended, it would be desirable to create a controllable, rapid decrease in material mechanical properties so that the object would fracture easily into small fragments, dramatically increasing the available surface area. In contrast, for objects which are uncontrolled in the environment, schemes (including autonomous chemically-based approaches driven by sunlight[7]) whereby innate mechanical properties are largely maintained while chemical degradation is enhanced would prevent harmful micro-fragmentation and enable the polymer to transition to carbon which is already present in large quantities in ocean environments.[8]

Polymer degradation processes are typically triggered by application of energy (*e.g.*, light or heat) that interacts with either (i) the surface of the material or (ii) homogeneously with the entire bulk. One strategy to alter the connection between mechanical stability and material deterioration is to initiate the degradation process from within the solid at well-defined, spatially-confined locations. Such an approach is possible by utilizing photothermal heating from nano-sized objects randomly embedded inside the polymeric material. For example, light resonant with the localized surface plasmon resonance (LSPR) of a metal nanoparticle is strongly absorbed[9–11] and rapidly converted into heat[12–14] which can then be utilized to drive thermal degradation, initiating in the immediate vicinity of each particle. One advantage of metal-nanoparticle mediated photothermal heating is that it requires matching of the incident light wavelength to the LSPR and thus can be intentionally triggered or avoided by altering the wavelength of light. During photothermal heating from a dilute concentration of nano-heaters, the sample experiences a steady-state spatially inhomogeneous temperature distribution.[14–18] Thus, material degradation is similarly spatially heterogeneous, leading to an alternative connection between mechanical response and chemical deterioration fraction. Light-to-heat conversion processes are also interesting in that they could potentially occur autonomously in the environment. Moreover, degradable materials may produce a permanent record of temperature exposure (such as creating locally degraded regions around each particle), which is potentially useful in characterizing the temperature field produced under nanoparticle-based photothermal heating.

In this work, photothermal heating *via* application of LSPR-resonant light to silver nanoparticles (AgNPs) contained within a polyethylcyanoacrylate (PECA) and starch composite is used to drive thermal degradation *via* a depolymerization pathway.[19–21] PECA is a useful material test system because it is industrially-relevant, has a single-step degradation pathway from polymer to monomer at relatively low temperatures (~150 °C),[20,22,23] and forms a fluorescent and electron-absorbing by-products upon significant degradation that manifestly reflect the photothermal heating field. AgNPs are utilized as a facile prototype nanoparticle: metal nanoparticle-based photothermal heating can be accomplished with many types of nanoscale objects.[10] Silver is less costly than the prototypically-utilized gold and forms an oxide layer. Understanding photothermal heating from oxidized silver may enable steps towards use of other oxide-forming (non-noble) metal nanoparticles. Myriad experimental techniques are utilized to monitor mechanical properties, chemical degradation, sample morphology on multiple size scales, and by-product formation under differing degradation conditions. The results indicate that driving degradation in an inhomogeneous manner creates mesoscopic pockets of low molecular weight material in the interior of a thin film. Bulk measurements of molecular weight and mass loss, when analyzed knowing the nanoparticle concentration within the sample, quantitatively agree with the results from completely-independent mechanical measurements and morphological observations. Highly degraded regions associated with each nanoparticle increase in size with laser intensity, resulting in a decrease in sample strength due to defect formation and thus altering the relationship between mechanical properties and fraction of chemical degradation as compared to the conventional, uniformly heated case. Formation of a pattern of an electron-absorbing material in the interior of degraded samples is discussed with regard to potential future applications.

2. Results and discussion

2.1. Fabrication of PECA : starch composite film

PECA serves as a model material system to demonstrate differences in thermally-activated polymer degradation and the associated changes in bulk properties and nanoscale morphology as a function of heating modality; *i.e.*, homogeneous heating *via* conventional means as compared with heterogeneous heating utilizing a photothermal approach from a dispersed low concentration of metal nanoparticles. Polymerization of ethyl cyanoacrylate (ECA) monomers to form PECA occurs at room temperature and can be initiated by any nucleophilic compound[24] including OH– ions within water,[25,26] which is the mechanism by which PECA acts as a common adhesive agent. A highly reproducible technique utilized acetone (an ECA solvent) as a miscibility agent to enable uniform mixing of a small quantity of water and the ECA.

Acetone volatilizes quickly and any remaining water can be removed by baking at a moderate temperature, which also ensures full completion of the PECA reaction and expulsion of residual ECA. An optimal mixture of 1 : 9 water : acetone by volume was adopted. Increasing the relative concentration of water decreases effective mixing with ECA; decreasing the water concentration removed the initiator. However, even under an optimized protocol, the mechanical properties of the resultant PECA were poor (highly brittle, as previously reported[20,27]) and the reaction time exceeded two hours. To resolve these concerns, 2 wt% starch[23] was added during polymerization. Adding a small amount of starch decreased the reaction time to ~1 hour, resulted in good tensile performance, and maintained high optical clarity (*i.e.*, transparency in the visible).

2.2. Effect of conventional heating: thermal stability and degradation

Fig. 1 displays isothermal mass loss measurements (filled purple squares) for PECA : starch samples after 1 hour in a laboratory oven. No weight loss was observed below 100 °C, indicating the absence of significant residual solvent within the polymer. Sample degradation occurs above ~150 °C and complete loss of mechanical stability (see below) as well as ~50% mass loss is observed at 200 °C. Isothermal mass loss *versus* temperature was consistent with a single thermally-activated decay mechanism, exponentially dependent on E_b/kT with an E_b barrier value of 27 kcal mol^{-1}. For comparison, a traditional TGA curve (black line) of a PECA : starch composite taken in air at the scanning rate of 10 °C min^{-1} is also displayed in Fig. 1. As discussed in greater detail in section 4.4 and consistent with the known degradation mechanism of PECA, TGA under nitrogen (dashed blue line) showed almost identical results to that under air.

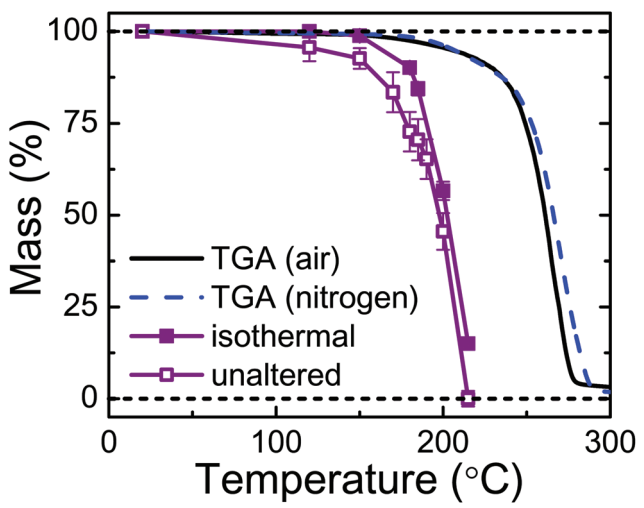

Fig. 1 Mass loss from PECA : starch composite under steady-state heating conditions for 1 hour (filled purple squares). TGA measurement in air (nitrogen) at a scanning rate of 10 °C min^{-1} is shown as a black (dashed blue) line. Unaltered sample mass estimates from a simple model are shown (open purple squares, see text for additional discussion). The difference between the open and filled squares at a given temperature represents the fraction of sample which depolymerized and then repolymerized rather than escaping the system.

The currently-accepted model of PECA degradation is chain unzipping (with an un-zip length approaching that of the chain length) from the initiated chain end which still contains the initiator, generating volatile monomer which must then diffuse out of the solid sample or risk repolymerization to form so called "daughter" oligomers.[20] Consistent with this model, thermal stability and degradation dynamics depend on initiator type[19,28] and in the solid state, on film thickness[22,29] (*i.e.*, polymer mass and surface-to-volume ratio). Previous work[22] found that barriers for PECA degradation increased from 15 kcal mol^{-1} for masses less than 15 mg (film thickness ~40 μm) where diffusion effects were negligible to 20 kcal mol^{-1} when the mass was quadrupled. Extrapolating the diffusion-limited data from that work to the mass utilized here (300 mg) results in an expected barrier of 31 kcal mol^{-1}, consistent with our result.

The molecular weight of PECA from PECA : starch composites as-made or after conventional heating for one hour at temperatures ranging from 120–215 °C was quantified *via* GPC. PECA : starch composite samples were dissolved in THF and the starch content filtered from the solution before measurement. A typical batch of as-made PECA has a weight-average molecular weight (M_w) in the range of 100k–300k g mol^{-1} and number-average molecular weight M_n of 50k ± 8k g mol^{-1}. The distribution in both as-made and heat-treated samples is bi-modal. Both the average molecular weight and polydispersity index (PDI, M_w/M_n) decrease with the increasing conventional degradation temperature. As shown in Fig. 2(a), the higher molecular weight species (corresponding to shorter retention time) completely disappears after conventional thermal treatment at 215 °C with the lower molecular weight (corresponding to longer retention time) component also narrowing slightly to result in one population (PDI = 1.5) of approximately 65 monomer-long chains. ECA and small oligomers of ECA are volatile species. One interpretation of the low molecular weight residue is that this represents the smallest non-volatile oligomer which is unable to escape from the sample under these experimental conditions.

To connect GPC results with isothermal mass loss data (Fig. 1), a simple model was utilized where the molecular weight distribution within the sample was represented by 20 chains: for instance, chain lengths ranging from 365 to 460 units corresponding to a Gaussian distribution with a central M_n of 51 616 and standard deviation of 7632 (consistent with the GPC data for an as-made sample). At each treatment temperature, chains were either removed (consistent with the chain unzipping model) or shortened to reduce the overall mass to the observed value. The resulting number averaged molecular weight could not match the experimentally-observed M_n values for any scheme which did not include a repolymerization process (*i.e.*, the retention of some fraction of the depolymerized monomers within the sample and a resultant formation of oligomers).

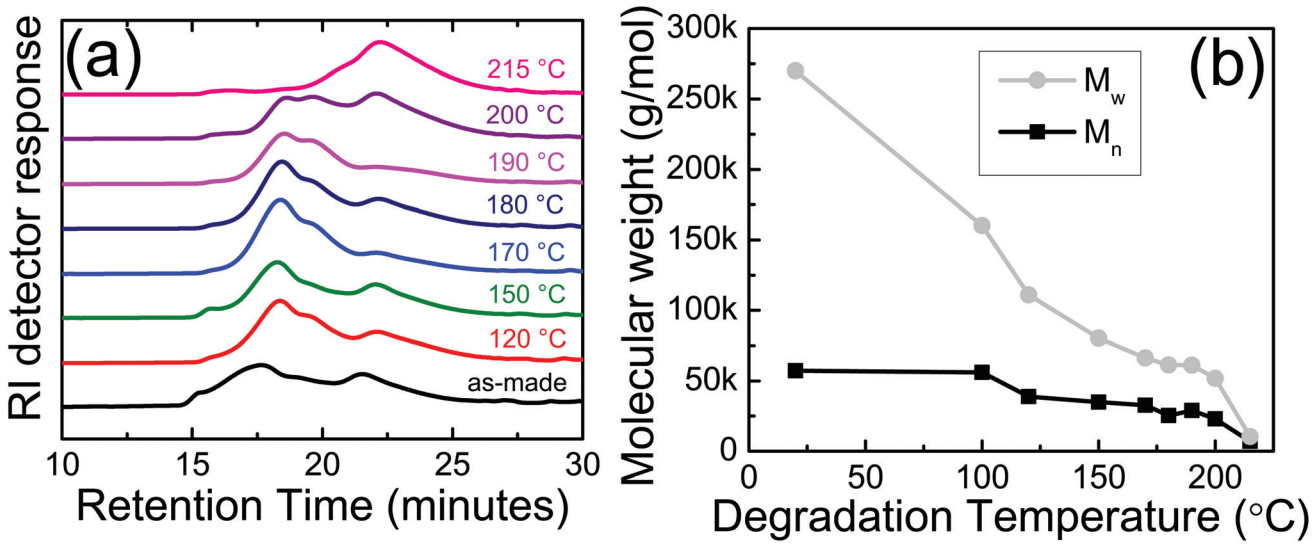

Fig. 2 (a) GPC curves of PECA : starch composite samples as-made or after conventional heating for 1 hour at steady-state temperatures between 120–215 °C. (b) Weight-average M_w and number-average M_n molecular weight obtained by GPC as a function of degradation temperature.

In other words, the mass loss and molecular weight data could not be reconciled without explicitly considering repolymerization. A scheme where mass decreased by removing entire chains and experimental molecular weight was obtained by removing additional chains and returning them as 60–70-mer (values consistent with the lower molecular weight peak in the GPC) enabled matching of both molecular weight and mass loss data for eight conventional treatment temperatures. In this interpretation, a large fraction of chains in the system are depolymerized (*i.e.*, fully un-zipped to form monomer). Some monomer diffuses out of the sample (or potentially forms volatile small oligomers) which results in reduction of sample mass. Other monomer repolymerizes in the film interior to form non-volatile "daughter" oligomers which changes the residual sample's average molecular weight but does not result in mass loss.

Fitting *via* the model then provides an estimate of the fraction of sample that depolymerized – a process that should be determined by an innate barrier, independent of the sample mass. Depolymerized mass estimates determined by this model are presented in Fig. 1 (open purple squares) and can be directly compared to experimentally measured isothermal mass loss values (filled purple squares). The difference between the open and filled squares at a given temperature represent the fraction of sample which depolymerized and then repolymerized rather than escaping the system. For example, after conventional treatment at 150 °C, the observed mass loss is less than 1%; however, the molecular weight analysis indicates that ~7% of the sample degraded, with the vast majority of this material unable to diffuse out of the sample and thus remaining to form non-volatile oligomers.

Plotting depolymerized mass estimated in this manner *versus* inverse temperature as shown in Fig. 3 enables determination of an expected barrier for depolymerization. As evident

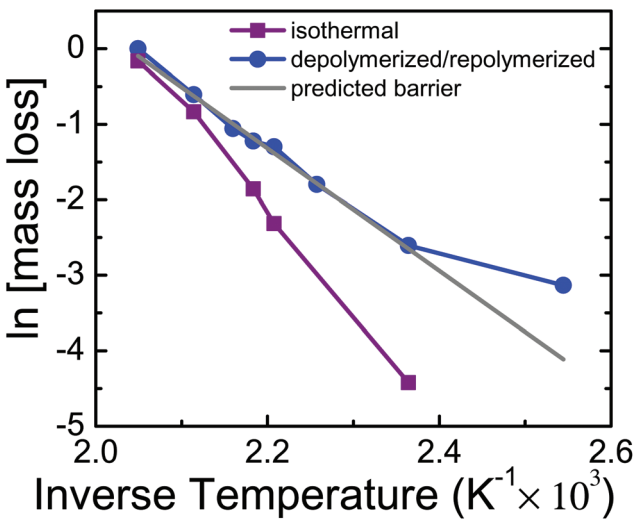

Fig. 3 Plot of natural log of relative mass lost from the sample (purple squares) and relative mass depolymerized (blue circles) *versus* inverse temperature. The fit (gray line) corresponds to a single Arrhenius process with a barrier to degradation of 16.1 kcal mol^{-1}.

from the graph, the estimated barrier for depolymerization is lower than the effective barrier for mass loss. The measured depolymerization barrier value of 16.1 kcal mol^{-1} is consistent with previously reported values (15.5 kcal mol^{-1}) for the innate degradation process. Thus, the data paints a clear picture of the thermally-driven deterioration process in macroscopic samples where long chains (polymer) are internally converted to short chains (oligomer) with some loss of mass from volatile products. These relatively unique polymer degradation properties make PECA an ideal system to study spatially-heterogeneous nanoparticle-based photothermal heating where the

warmest regions are deep within the sample, thus further minimizing diffusion through the cooler surrounding material and potentially enabling transformation of the sample from polymer to oligomer with limited mass loss.

2.3. Effect of conventional heating: mechanical properties

Prototypical stress–strain curves for as-made and highly-degraded PECA : starch samples demonstrate a brittle fracture (see ESI Fig. S1†). Fig. 4 summarizes stress at break, strain at break, and modulus changes as thermal degradation proceeds after conventional heat treatment for one hour. Plotted data from both PECA : starch (closed symbols) and PECA : starch : AgNPs (250 pM, open symbols) are self-consistent, indicating that the incorporation and presence of the AgNPs has no significant effect on the mechanical properties of the PECA : starch composite.

The fracture strength as a function of treatment temperature is plotted (blue circles) in Fig. 4. Generally, in the early stages of any degradation, the shortening or removal of chains creates weak points (*e.g.*, defects) at random locations throughout the sample. Such defects lead to decreased strength (*i.e.*, failure at lower applied stress) because they act as local stress concentrators: that is, the applied force is divided among fewer chains than in intact regions of the sample. This overall trend is evident at thermal treatment temperatures above ~100 °C as sample strength decreases and continues until samples can only support 3 MPa (which is ~11% of the original value) after being exposed to 190 °C. For treatment temperatures above this level, tensile data could not be obtained as the sample crumbled upon loading into the testing apparatus. In concert, maximum strain at break (Fig. 4, black squares) also decreases as the sample cannot elongate significantly without encountering a defect, consequently leading to breakage at lower strains.

The glass transition temperature T_g of PECA is ~150 °C.[30,31] Thus when the room temperature tensile measurements are conducted, the sample is a glassy material and defect size can be estimated from the classic analysis[32] in which the breaking stress σ_b is related to the modulus E as:

$$\sigma_b = \sqrt{\frac{2E\gamma}{\pi\nu a}} \quad (1)$$

where γ is the surface tension, ν is Poisson's ratio, and $2a$ is the characteristic size of the defect. The as-made material has a characteristic innate defect size, estimated[33,34] by using γ = 34 mJ m^{-2} and u = 0.35 to be $2a$ = 270 nm. Based on the experimentally-observed strength after exposure to elevated temperatures the characteristic defect size increases to a few microns. This range of values is consistent with expectations for a polymeric material. These defect sizes will be compared with those generated as a result of heterogeneous heating (see section 2.5).

The tensile modulus (Fig. 4, green triangles) is constant for treatment temperatures up to 170 °C above which a dramatic decrease is observed. Because the modulus quantifies the response to small perturbations and thus is insensitive to defect formation, values are typically maintained through early stages of degradation and only decrease when the molecular weight has fallen significantly, particularly below twice the entanglement molecular weight.[35] The critical molecular weight M_C for PECA can be estimated from Wool's approximation[35] using values reported in the literature, yielding 34 300 g mol^{-1}. M_n after heating at 170 °C is approximately this value (32 700 g mol^{-1}), and falls to 25 400 g mol^{-1} after thermal treatment at 180 °C (the next data point in the sequence, Fig. 2(b)). From analysis of the area under the bimodal peak in the 180 °C GPC data (Fig. 2(a)), 40% of the chains are below M_C even though M_w is still 61 000 g mol^{-1}. Treatment at 215 °C results in M_w = M_n = 7050 g mol^{-1}. Thus, after 1 hour of degradation in the temperature range 180–200 °C, the system reaches the critical molecular weight and significantly weakens due to the lack of an entangled network. Because the modulus is a valuable tool to track degradation late in the process when the molecular weight is small, it will also be utilized in understanding the mechanical differences resulting from photothermal heating in section 2.5.

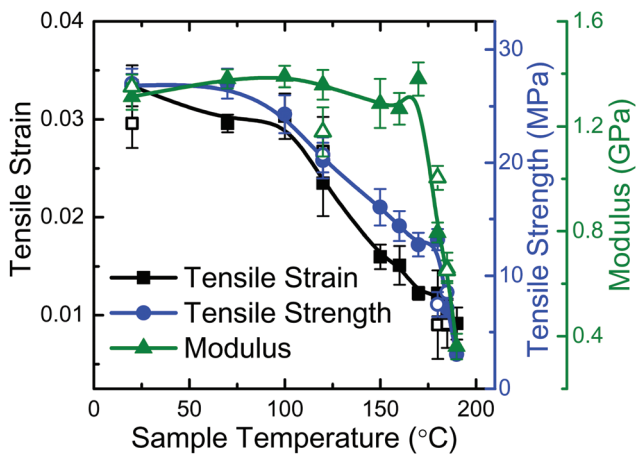

Fig. 4 Tensile strain at break (black squares), strength at break (blue circles), and modulus at low strain (green triangles) are presented for both PECA : starch (filled symbols) and PECA : starch : AgNPs (250 pM concentration, open symbols) composite samples.

2.4. Effect of conventional heating: sample morphology under degradation

Fig. 5(a) is a characteristic bright field image of an as-made PECA : starch composite sample. It reveals a mostly featureless surface, with small scratches present which are likely produced in the fabrication process. Fig. 5(b) is an identical, as-made sample where the starch has been dyed to provide contrast in the image, illustrating the size and spatial distribution of the starch granules and demonstrating that over the few micron depth of field, multiple levels of starch can be visualized. The number of starch particles observed is consistent with the intended loading level (2%) and the average granule size. As the sample degrades, the primary morphological changes observed *via* optical microscopy are bubble formation at inter-

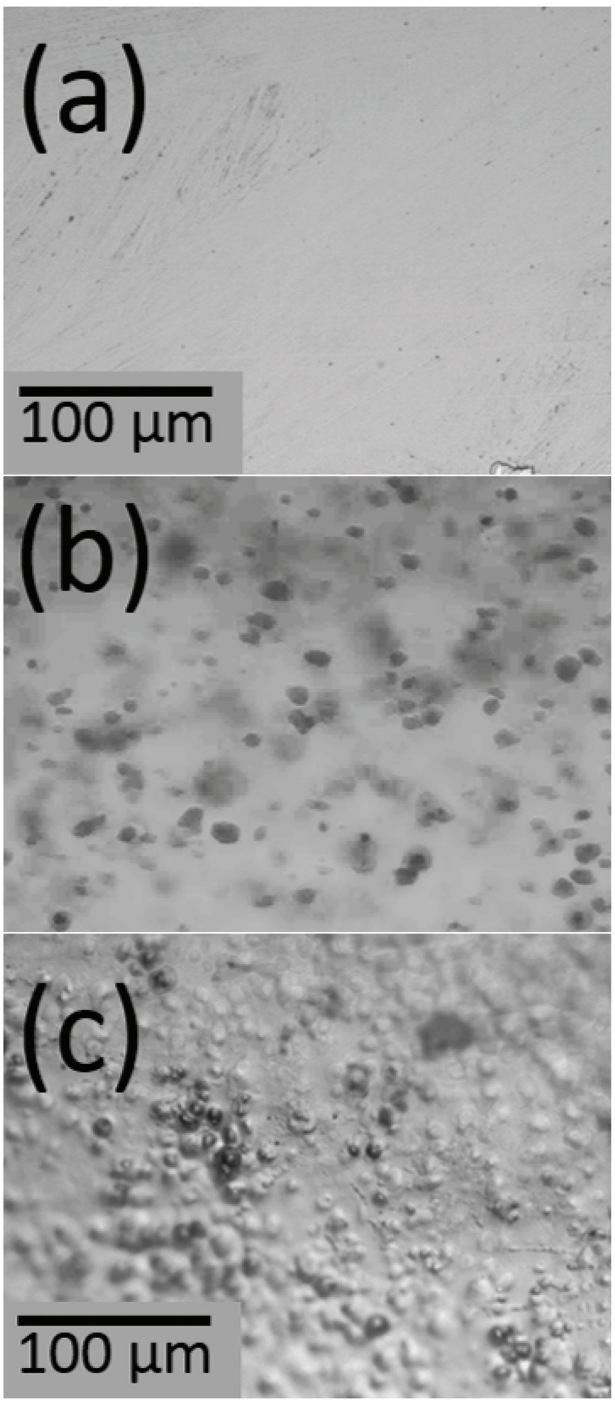

Fig. 5 (a) and (b) Bright field images of as-made PECA : starch film samples where the starch in the film presented in (b) has been intentionally dyed so as to appear dark; (c) after 1 hour conventional treatment at 215 °C where exposure of starch granules at the surface due to loss of PECA is evident. The scale is the same for all images.

mediate temperatures and exposure of starch as the surrounding surface PECA is removed. For instance, treatment at 215 °C results in complete depolymerization and 85% mass loss, thus a much higher fraction of the remaining material are starch granules, as shown in Fig. 5(f). SEM images also confirm the presence of starch at the surface as shown in ESI Fig. S2.† Granules can be faintly observed under the PECA in as-made samples and are fully revealed in 200 °C thermally-treated samples (which have lost 44% of their original mass, the vast majority of which should be PECA).

As discussed in the Experimental Methods section, both PECA and starch develop degradation-induced luminescence after exposure to elevated temperatures. Starch is non-volatile and becomes luminescent after experiencing a temperature greater than 140 °C for one hour, which is the dominant feature of fluorescence microscopy images of conventionally-treated samples as shown in ESI Fig. S3† (excitation 350–400 nm, emission collection over 450–500 nm, additional details appear in section 4.4).

While optical imaging and SEM morphology are dominated by starch granules at or near the sample surface, transmission electron microscopy (TEM) predominantly probes the regions between starch granules, which are generally featureless in as-made samples. Optical images (*e.g.*, like Fig. 5) confirm that spheroidal starch granules have a distribution of sizes ranging from ~1–20 μm in diameter. Starch is well-separated in as-made samples with open starch-free regions that are also in the 1–20 μm size range, which is consistent with the characteristic image field sizes for TEM, generally one to a few microns square. This spatial scale (10 nm–10 μm) is the most important for determining the effects of photothermal heating and TEM probes the sample's interior morphology by imaging microtomed 100 nm thick slices. Thus, it will be the focus of the morphological studies for the remainder of this report.

Fig. 6(a) and (b) are TEM images of 100 nm thick microtomed slides of as-made PECA : starch : AgNPs, where the dark, quasi-spherical objects are AgNPs. Two images are presented to show the variation in AgNPs and PECA appearance for different samples taken under slightly altered imaging conditions. As discussed in sections 2.5 and 4.2, the observed number of AgNPs in as-made samples is consistent with expectations. At this highly-dilute concentration (~35 pM) most TEM images of random sample regions contain no nanoparticles.

The most significant morphological observation from TEM images of conventionally-heated PECA samples is the discovery of electron-absorbing regions (*i.e.*, unexpected dark spatial features in the electron micrographs) due to polymer degradation. This finding is consistent with the formation of a luminescent compound due to degraded PECA, which has been previously associated with amorphous carbon and/or interactions between conjugated carbonaceous groups.[36] Fig. 6(c)–(f) are characteristic images from PECA : starch samples that have been degraded for 1 hour at different average temperatures. The results of thermal-treatment at 150 °C [195 °C] is shown for Ag-free PECA : starch (Fig. 6(c)) [Fig. 6(e)] and for PECA : starch : AgNPs (Fig. 6(d)) [Fig. 6(f)] samples, respectively. The observed sample morphology is completely consistent for all PECA : starch samples with or without AgNPs after experiencing the same conventional heating conditions. Specifically, all degraded PECA samples show small dark regions that tend to be connected into longer chains or pat-

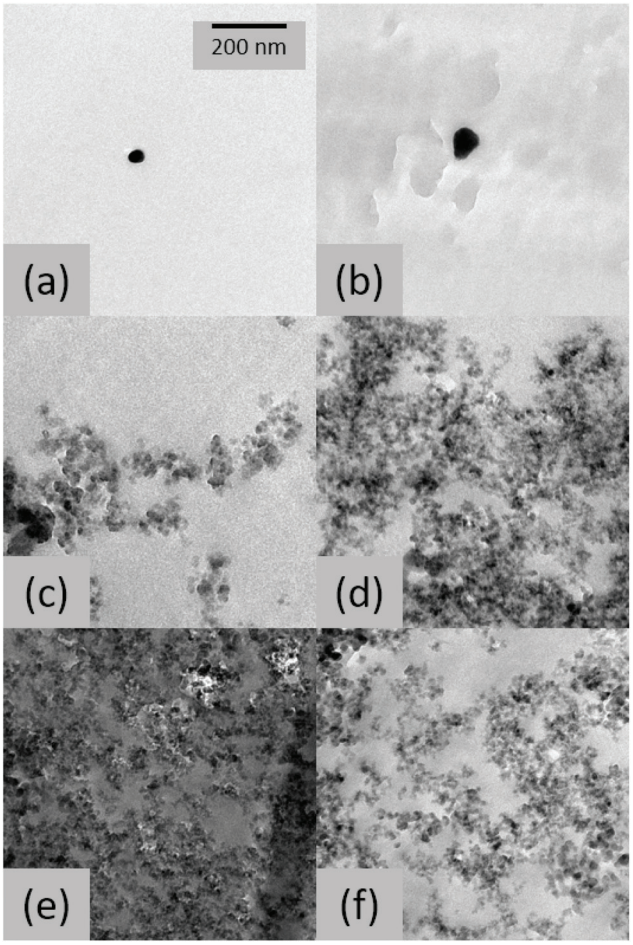

Fig. 6 (a) and (b) TEM images of micro-tomed slices of as-made PECA : starch : AgNPs. TEM images of samples after thermal treatment for 1 hour of (c) [(e)] Ag-free PECA : starch sample degraded at 150 [195] °C, to compare with (d) [(f)] a PECA : starch : AgNPs sample having experienced the same conditions. Scale bar shown in (a) is the same for all images.

terns. The fraction of such electron-absorbing material does not change significantly with treatment temperatures over 180 °C, which is consistent with its identification as a non-volatile degradation by-product within the PECA depolymerization reaction which primarily forms volatile products. A recent publication[37] reported fabrication of nitrogen-doped graphene from PECA degraded at elevated temperatures (600–1000 °C). Those authors proposed a mechanism whereby formation of aromatic cyclic structures (containing both nitrogen and carbon) and de-esterification (*via* removal of H from sp^3 carbons to form carbon–carbon double bonds) occurred between 160 and 300 °C as precursor steps towards graphite-like materials at higher temperatures, which is consistent with our observations.

For the purposes of studying photothermal heating, this side-reaction is useful to show the heterogeneous heating pattern where, as discussed below, electron-absorbing material only forms in the immediate vicinity of AgNPs under photothermal heating. Photothermal heating, in turn, is then also useful for understanding the process leading to such non-volatile side products.

2.5. Effect of photothermal heating: mass loss, molecular weight, and mechanical properties

TEM images confirmed the presence of ~50 nm diameter AgNPs consistent in size and shape with AgNPs drop-cast from solution and relatively well-dispersed within the PECA : starch material. The effective concentrations of the nano-heaters (*i.e.*, either as individual nanoparticles or small clusters of particles) for the two different loading levels were 35 and 250 pM (as discussed further in section 4.2). These values are within a factor of 2 of the expected concentration given perfect dispersion of mono-size AgNPs and result in an average inter-heater distances of 4.5 and 2.3 μm, respectively.

PECA : starch : AgNPs composite film samples were photothermally-heated with 445 nm continuous-wave light that overlaps the AgNPs LSPR (which peaks at ~434 nm). As described in section 4.3, a combined laser system irradiated the entire gauge length 8 mm × 30 mm region utilized in mechanical measurements at an average intensity of up to 1.5 W cm^{-2} for one hour. Film samples containing 250 pM of AgNPs which were photothermally-heated for 0.5 hours with a light intensity of 1.5 W cm^{-2} experienced total degradation (*i.e.*, complete loss of mechanical stability to the extent that post-treatment tensile measurements were not possible). For the other cases, the average sample temperature was determined by use of an embedded molecular fluorophore, as discussed in section 4.6, and ranged from 30 to 185 °C, depending on both laser intensity and AgNPs concentration. PECA : starch samples without AgNPs experienced a small amount of non-specific laser absorption; however even in an extreme illumination condition (1 hour at 1.0 W cm^{-2}) the resultant average sample temperature was less than 35 °C.

Photothermal heating from a dilute concentration of nanoparticles within a solid polymeric material produces an inhomogeneous temperature distribution where the temperature near a particle is significantly warmer than the background.[15,16,38–40] For the molecular fluorescence thermometry technique employed here the fluorophores are uniformly present throughout the sample and each individual's emission reflects its local environment. The resultant ensemble fluorescence spectrum can be analyzed to determine a volume-averaged sample temperature. Under the heterogeneous heating utilized in this work, the warm region around each particle represents a small fraction of the overall sample volume, therefore the average sample temperature is generally close to the coolest temperature in the system. Thus when comparing samples heated photothermally and conventionally to the same average temperature, the observed difference will primarily be due to the effects of the local hot regions in the small volumes surrounding each photothermal heater.

Fig. 7 summarizes mass changes experienced under photothermal (red circles) and conventional (purple squares) heating. An interplay exists between the local temperature

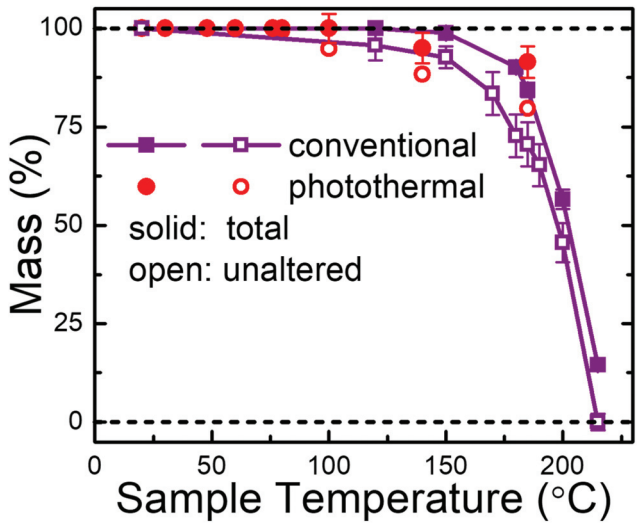

Fig. 7 Mass of the sample after experiencing a selected average temperature for 1 hour under uniform conventional (purple squares, same data from Fig. 1) or heterogeneous photothermal (red circles) heating. The filled symbols represent the total amount of the remaining sample; the open symbols depict the fraction of the sample which remains unaltered (*i.e.* in its original state without experiencing a depolymerization/repolymerization transition).

which drives the degradation process, the overall spatial temperature distribution which determines which parts of the sample will deteriorate, and the ability of the degraded material to escape the sample or if unable, to repolymerize into a lower molecular weight (*e.g.*, oligomer) form. Generally the heterogeneous spatial temperature profile generated *via* photothermal heating results in a flatter response with average sample temperature (Fig. 7, filled red circles) as compared to conventional heating (Fig. 7, filled purple squares): that is, the unzipping process starts at lower average temperatures and is less extreme at higher average temperatures.

Photothermally-heated samples with average temperatures <100 °C showed no mass loss, because the minute fraction of the sample potentially reaching degradation temperatures is predominantly confined within the sample's interior. As nanoparticle concentration and/or light intensity is increased, the fraction of the sample experiencing elevated temperature grows, due either to the presence of additional heating objects or a larger "hot" region around each particle. These changes also result in an increased average sample temperature. For average temperatures in the range of 120–150 °C, a substantial fraction of the sample is above the expected degradation temperature and thus these cases show enhanced mass loss compared to analogous uniform conventional heating to the same average temperature. For instance, for the 250 pM, 0.6 W cm^{-2} treated sample (average temperature 140 °C) mass loss is ~5× that of the 140 °C conventional case.

When the average temperature is significantly above the 120–150 °C range then most sample material is experiencing temperatures that lead to degradation and the mass loss under photothermal heating is comparable with, or slightly lower than, the equivalent case under uniform conventional heating. This observation makes sense because the warmest regions of the photothermally treated sample, in particular where the material is experiencing >185 °C, are in the interior where even significant heating may result in only small mass loss due to the limited diffusion rate of liberated monomer. Hence, the degraded and volatile material cannot easily escape from the sample. In contrast, mass loss readily occurs at the surface regions, which are on-average slightly cooler than the average temperature.

Photothermally-heated PECA : starch : AgNPs samples experiencing average temperatures >80 °C showed changes in measured molecular weight; thus, a depolymerization fraction of the sample mass could be estimated using the previous discussed simple model (see sections 2.2 and 4.4). In Fig. 7, the estimated fraction of the sample which remains in its unaltered state as a function of treatment temperature is shown for photothermal (open red circles) and conventional (open purple squares) heating. Hence, for each heating modality, the difference between the 100% mass level (dashed horizontal line) and the solid data symbols represent the sample mass which has depolymerized into volatile degradation products and was able to escape the sample. The difference between the solid data symbols and the open data symbols represent the fraction of the sample which thermally deteriorated but was unable to diffuse sufficiently rapidly to leave the sample before repolymerizing, thus remaining but with a lower molecular weight (*i.e.*, a repolymerized oligomer). In general, photothermal depolymerization fractions follow the mass loss trends.

As the heterogeneous temperature field due to the dispersed nanoparticle heaters is driving the degradation reaction, depolymerized material may be localized in regions around each nanoparticle or nanoparticle cluster, particularly at lower average temperatures. Therefore, the depolymerized fraction can be translated to an average depolymerized size scale. Utilizing the effective heater concentration, the average depolymerized volume per heater and the equivalent average depolymerized radius was determined. This estimated depolymerized size scale, resulting from the observed mass loss and molecular weight measurements, is plotted as a function of temperature in Fig. 8(a) (red star data).

Comparing analysis of mass loss and molecular weight measurements with the results of tensile testing provides insight into the morphology of the sample under photothermal degradation. At average sample temperatures <60 °C or >180 °C, mechanical properties from photothermal heating match the conventionally heated case at the same average temperature as shown in Fig. 8(b) which plots stress at break. In contrast, for the moderate temperature region where degradation is significant but not complete, the mechanical properties of photothermally heated samples (blue symbols) are always weaker (*i.e.*, a lower stress and strain at break) than their counterparts which were conventionally heated at the same average temperature (black squares).

As discussed in section 2.3 tensile stress at break is limited by defect size. Thus decreased strength after photothermal

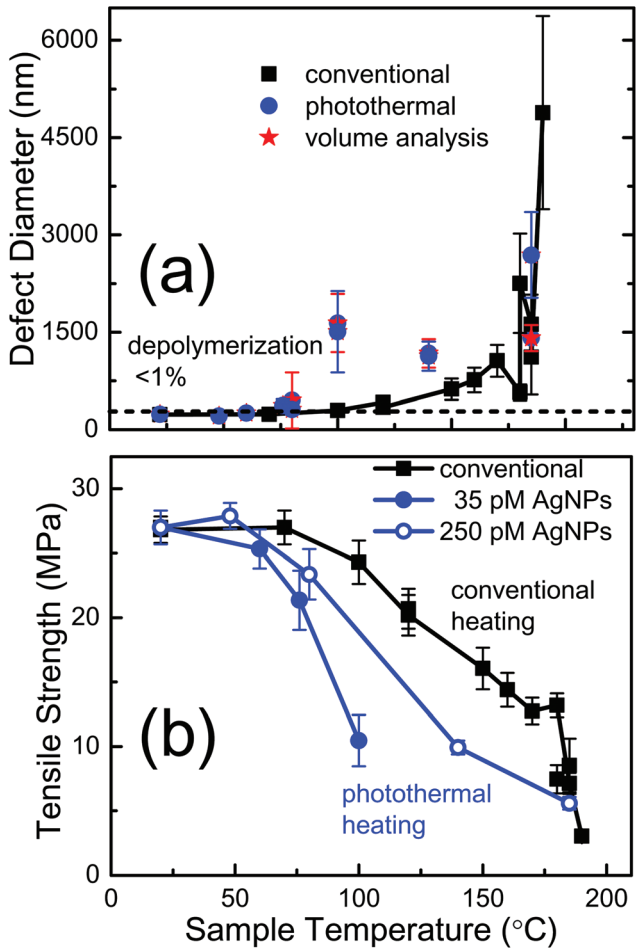

Fig. 8 (a) Estimates of the average defect size within degraded samples as a function of treatment temperature from either depolymerization volume analysis (red stars) or from mechanical measurements (blue circles for the photothermal case, black squares for the conventional case) under different heating modalities. The dashed line represents the intrinsic defect size in as-made samples. (b) Tensile strength at break *versus* average sample temperature under conventional (black squares) or photothermal heating containing 35 pM (filled blue circles) or 250 pM (open blue circles) of AgNPs.

heating indicates that new or enlarged defects are being formed. Inverting eq. 1, the observed tensile stress and modulus can be used to estimate the characteristic defect size, presented in Fig. 8(a) for both photothermal (blue circles) and conventional (black squares) heating. In this analysis, the lower observed stress at break is represented as a larger defect size. The average radius of the depolymerized region around each heater (red stars) in Fig. 8(a) is consistent with the defect size determined from mechanical measurements. Note that these estimates originate from completely independent measurements: the depolymerization diameter (red stars) reflects the mass loss and molecular weight results whereas the defect diameter (blue circles) is determined from tensile testing.

Overall, this result indicates that the depolymerized material, which either repolymerizes as oligomer or diffuses and escapes from the sample, results in the creation of localized defects around each photothermal heating site. Thus, focusing the degradation in specific locations rather than homogeneous spatial degradation throughout the material fundamentally alters the relationship between chemical and mechanical properties, which was one goal of this work. As discussed in the introduction, such relationships are important because they determine whether a material stays intact or forms fragments at different points during the degradation process.

Fig. 9 summarizes the relationship between chemical degradation (*e.g.*, depolymerization fraction or the fraction of the sample that has degraded) and mechanical properties (*i.e.*, the tensile stress at break). The number indicated near each data point is the average temperature at which the sample was degraded. The black square symbols reveal the mechanical-chemical correlation under conventional degradation: the tensile properties decrease until 5–7% chemical degradation, and then are relatively stable in the range 7–27%. Above this, a steep decline is observed until loss of all mechanical integrity (above ~35% degradation fraction). In contrast, photothermal heating (blue symbols) leads to significantly weaker samples even at 5% degradation and samples are barely intact at 20%, which is consistent with formation of defects in the sample interior due to heterogeneous degradation. For instance, for photothermally-treated samples having experienced an average temperature of 100 °C, which would have no effect if applied uniformly under conventional heating, 5% of the sample chemically degrades but the mechanical properties are consistent with conventional treatment at 180–185 °C. Note that the data in Fig. 8(a) indicates that this 5% of the sample volume, distributed uniformly to each heating element, results in a

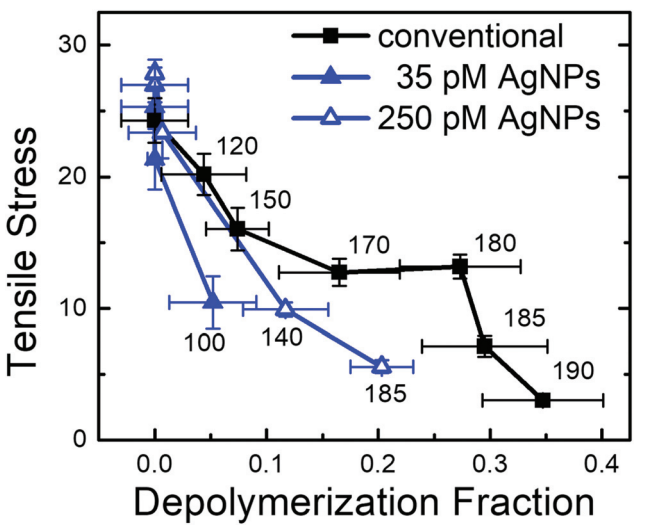

Fig. 9 Measured tensile stress at break *versus* the fraction of the sample that has depolymerized for conventionally (black squares) or photothermally (250 pM AgNPs, open blue triangles; 35 pM, filled blue triangles) treated samples. The average temperature for each degradation condition in °C is annotated near the associated point.

depolymerization radius consistent with the defect size approximated from the observed mechanical properties. Thus, the reason why a photothermally heated sample treated at 100 °C has the same stress at break as a 185 °C conventionally-heated sample is because they contain defects of a similar size.

While the strain at break follows a similar trend as the stress at break (compare Fig. 4), as discussed in section 2.3, the modulus provides independent information about the molecular weight of the sample. Samples treated photothermally or conventionally at 185 °C had identical mechanical properties, including a decrease in modulus. This result indicates that photothermal heating can drive the degradation process to the point where the dominant chain length in the system has significantly decreased. Photothermally-treated samples that experienced average temperatures of 140 °C also showed a decreased modulus (890 ± 35 MPa), in contrast with the corresponding conventionally-treated case which retained the as-made modulus of ~1300 MPa. In this thermal treatment temperature range, the photothermally treated samples have a higher depolymerization fraction than the conventional analog (see for instance, Fig. 9, comparing the conventionally-treated 150 °C sample and the photothermally-heated 140 °C sample), which is consistent with a lower modulus.

2.6. Effect of photothermal heating: morphological changes

Examining the morphology of photothermally-treated samples also revealed effects of the heterogeneous temperature distribution. Fig. 10 contains TEM images to characterize internal sample morphology (*i.e.*, the PECA located between starch granules). For as-made samples which have experienced a maximum temperature during fabrication of 65 °C, images in Fig. 10(a) and (b) reveal a mostly featureless sample where the striations are due to the micro-toming process. These images contain a few AgNPs (circled in red) in (a) and an unusually large AgNP (with a diameter of ~100 nm where the average is 50 ± 10 nm) in (b) to provide a size scale. Other images of AgNPs in as-made samples were previously presented in Fig. 6(a) and (b).

Fig. 10(c) and (d) TEM images summarize morphology of PECA : starch samples with 35 pM AgNPs concentration treated with 0.6 W cm^{-2} light intensity for 1 hour, resulting in an average sample temperature of 76 °C. Under this thermal treatment, samples revealed little gross effect: no mass loss or depolymerization was observed and mechanical properties were not significantly changed compared to as-made samples. However, larger electron-absorbing features (*i.e.*, black regions that are not AgNPs) are noticeable in both TEM images; analysis of twenty low magnification images identified 18 dark objects, 10 of which could clearly be classified as silver nanoparticles or clusters of silver nanoparticles. The remaining eight objects were larger than a characteristic nanoparticle and had a more-layered appearance, with an average diameter of 180 ± 20 nm. Fig. 10(e) and (f) present TEM images of samples with the same low AgNPs concentration, treated with a higher laser intensity (1 W cm^{-2}), which subsequently experienced an average temperature of 100 °C, and had an estimated 5% depolymerization. For this case, only 3 of 13 objects in 20 large-scale images were consistent with "neat" AgNPs (as appearing the as-made samples) and the average size of the new features was 215 ± 45 nm. Note that for conventionally heated samples, no change in sample morphology is expected for these cases.

Fig. 10(g)–(j) summarize a continuation of the sequence of experiments but with a higher (250 pM) nanoparticle concen-

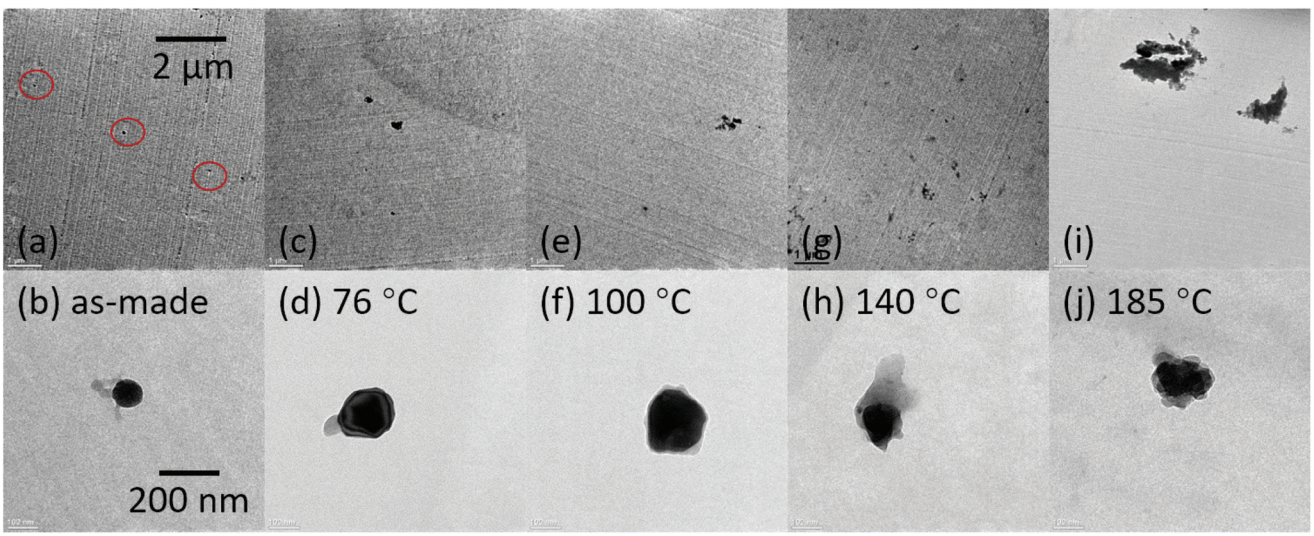

Fig. 10 TEM micrographs of micro-tomed 100 nm thick slices of PECA : starch : AgNP after photothermal heating to selected average temperatures. Top row: Low magnification 8 μm × 8 μm images; bottom row: high magnification 880 nm × 880 nm images. Scale bar is given in the first image and is the same for each row. (a) As-made: AgNPs are circled in red; (b) as-made: a particularly large AgNP is presented; photothermally treated: (c)–(j) carbonaceous material associated with PECA degradation is produced in the vicinity of each AgNP upon photothermal heating. This degradation by-product material appears as large black objects under TEM analysis.

tration, resulting in increased average sample temperatures of 140 and 185 °C, respectively. Fig. 10(h) and (j) can be directly compared to the conventional analogs in Fig. 6(c)–(f). From such an analysis, it appear that the electron-absorbing PECA degradation product that manifests as 10–20 nm features distributed in clusters or chains throughout the conventionally-heated samples is instead focused in spherical regions, which are presumably centered on AgNPs as this is the hottest spatial region in the material. This hypothesis is consistent with the lack of "neat" silver nanoparticles within the TEM images, as the AgNPs cannot be visualized behind the electron-absorbing degradation product formed around them. In particular, in symmetry with the lower concentration, after treatment with 0.6 W cm^{-2}, only 50% (15 out 30) of the dark objects in TEM analysis are consistent with "neat" AgNPs and the average diameter of the PECA-degradation-related features is 200 ± 20 nm. For the highest temperature case (250 pM concentration illuminated with a light intensity of 1.0 W cm^{-2} creating an average sample temperature of 185 °C) of the 25 features identified in the TEM analysis, none could be classified as nanoparticles and the average dark feature diameter was 450 ± 45 nm.

In photothermal heating from a dilute concentration of nano-objects, the temperature profile in the immediate vicinity of the particle will depend primarily on the laser intensity and be relatively independent of the background temperature. Re-examining Fig. 10 in this context, for the lower intensity (2^{nd} and 4^{th} columns) features of a characteristic size appear and the primary difference in the two images is the number of dark spots (as the concentration of particles increases by 7×). This idea is consistent with the features having similar average diameters (see above and section 2.7) and the frequency (about 50%) of intact AgNPs. As the illumination intensity increases, the temperature at a given distance away from the nano-heater should increase, which results in a larger degraded PECA by-product region, assuming this reaction is driven by a characteristic temperature. As discussed in section 2.7, the physical size of the presumed luminescent and electron interacting degradation by-product formation shown *via* TEM is significantly smaller than the estimated "hot region" around each particle as determined by other methods. Given that under conventional heating, the by-product forms at temperatures as low as 140 °C, which is within the temperature range where the other experiments are also sensitive, a smaller observed radius indicates that multiple factors such as confinement of degraded products or multiple depolymerization–repolymermzation cycles as well as high temperature are required to produce this compound. Note that for higher concentration samples (Fig. 10(g)–(j)), the background temperature is sufficiently high to create the degraded PECA by-product away from the AgNPs locations and thus additional detailed analysis is difficult.

Most of the proceeding analysis of photothermal samples has focused on the cases where average temperatures are the highest (ranging from 76–185 °C) and thus the development of defect sites affects mechanical properties, mass loss or molecular weight change are observed, and/or features in TEM can be clearly distinguished from AgNPs. For samples experiencing lower average temperatures, photothermal activity is still present but only affects a minute fraction of the sample. The fortuitous observation that starch becomes luminescent after degradation enabled use of optical imaging to illustrate these effects.

Fig. 11(a–d) shows characteristic fluorescence microscopy images for photothermally-heated samples that experienced average temperatures of 48–100 °C. Images reveal the presence of isolated bright spots which are identified as starch. At these bright locations, the local temperature has exceeded 140 °C. Fig. 11(e) summarizes the number of luminescent starch granules as a function of photothermal laser intensity and particle concentration. The average temperature is annotated on each point. The horizontal line is the total number of starch granules in the image field. For photothermal treatment conditions that resulted in average sample temperatures greater than 140 °C, all particles were luminescent, and the images were very similar to the conventional analogs (see ESI Fig. S3†).

For each optical image, the predicted number of AgNPs in the image field is ~8600 (~61 400) for 35 (250) pM, respectively. This insight makes it evident that a relatively unusual event leads to development of a sufficiently intense "hot spot" and consequently results in starch degrading and becoming luminescent. We hypothesize that coincidental overlap a starch granule and two heated regions (each arising from an individual AgNPs or small cluster of AgNPs) creates a particularly warm location and analyze the data in this light.

A revealing aspect of the image sequence and analysis in Fig. 11 is that the number of bright features is not proportional to the average temperature. Fig. 11(a) is from a sample that experienced an average temperature of 48 °C during photothermal heating (250 pM AgNPs concentration irradiated with 0.3 W cm^{-2} intensity) and is the lowest intensity point in Fig. 11(e). A lower concentration sample (35 pM AgNPs) treated at a higher intensity (0.45 W cm^{-2}) experienced a significantly higher average temperature of 60 °C but displayed no bright spots (data not shown). In fact, the lower concentration samples (black points in Fig. 11(e)) consistently have fewer luminescent starch observations than high concentration samples (blue points) independent of the average temperature. Presumably the lower concentration results in fewer opportunities for a coincidental overlap of the heated regions around each particle. To illustrate this point, compare the conditions shown in Fig. 11(b) and (c) which have similar average temperature but an average of 1.5 bright spots for 35 pM case while the 250 pm case has about 9 spots per image. Thus, there is no simple correlation between the average temperature and number of bright spots observed. In contrast, the results are consistent and predictable when analyzed in the light of the number of hot regions (effective AgNP concentration) and can be utilized to roughly estimate hot region diameter.

The number of intersections (bright regions) depends on the AgNPs concentration but also on light intensity (for example, the number of overlapping regions tripled for the

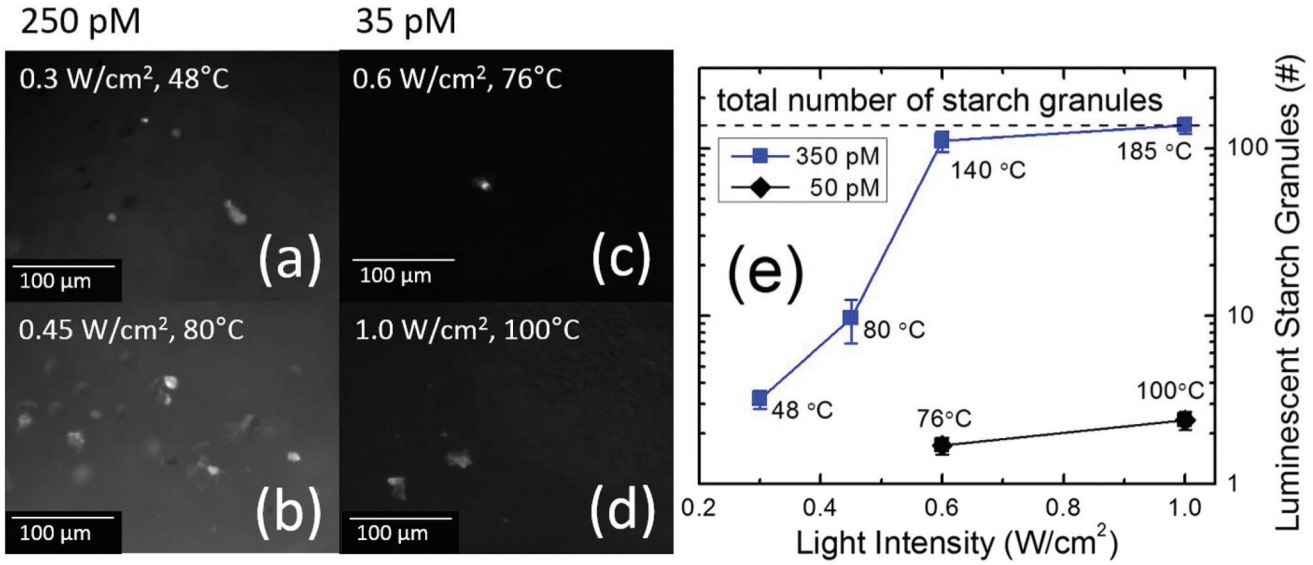

Fig. 11 Fluorescence microscopy images of PECA : starch : AgNPs samples having (a), (b) 250 pM or (c), (d) 35 pM AgNPs concentration. Illumination intensity and the resultant average temperature under photothermal heating are stated on each image. The bright regions are starch rendered luminescence through degradation by experiencing a local temperature >140 °C. (e) Number of luminescent starch granules observed in fluorescence microscopy (image size 329 × 248 μm with a field depth of approximately 5 μm) of photothermally treated samples *versus* intensity of the light utilized for photothermal heating for two different AgNPs concentrations. For each case a sufficiently large number of images was obtained so that between 25 and 150 events were observed. The average temperature of each sample is noted. The horizontal dashed line indicates the available number of starch granules (dark or luminescent) in the sample as determined by analyzing images of as-made samples with intentionally-dyed starch (see Fig. 5b). For treatment temperatures at or above 140 °C, all starch particles are luminescent. Below this value, the number of bright starch objects is used to estimate the size of the "hot region" around each particle, as discussed in the text, and summarized in Fig. 12.

lower concentration samples when the intensity rose from 0.6 W cm^{-2} to 1 W cm^{-2}). Increased illumination intensity should enlarge the size of the effective "hot volume", that is the region around each particle where temperatures are significant enough that overlap with another hot region would result in a local temperature greater than 140 °C. The characteristic size of this "hot volume" can be estimated from the fluorescence data as follows: the average number of overlaps should be proportional to (i) the volume fraction of starch, (ii) the volume fraction of the hot regions squared (as two hot zones must overlap) and (iii) the number of "sites" in the system (sample volume/hot region volume, as the hot region is now the smallest volume in system). Modeling the hot volume as a spherical region, for the four cases summarized in Fig. 12, such analysis can be utilized to estimate the hot region radius as a function of intensity. These values, presented in a Fig. 12 as circle symbols, increase monotonically with intensity (independent of concentration) and range from 200–500 nm, the same order of magnitude as the other estimates of hot region radius (*e.g.*, 125–750 nm, from depolymerization (square symbols)) for these experimental cases.

2.7. Effect of photothermal heating: temperature distribution

Fig. 12 summarizes the experimental estimates of the size of heated region around each nanoparticle as determined in this work. For reference, recall that the average AgNP radius is 25 nm and that the distance between particles is either 2.4 or 4.4 microns, depending on concentration. As discussed above,

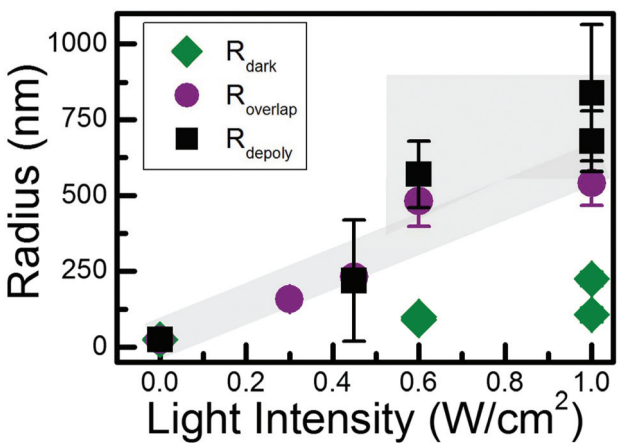

Fig. 12 Summary of estimates of the "hot region" around each nanoparticle as a function of intensity of photothermal heating light from the depolymerization fraction (R_{depoly}, square symbols), analysis of luminescent starch in optical imaging ($R_{overlap}$, circle symbols) and the size of the electron-absorbing degradation by-product around each particle as evidenced by TEM (R_{dark}, diamond symbols). The zero intensity value is set to the radius of the nanoparticle (25 nm). Multiple points of a particular type at each intensity are due to the different concentrations, with the higher concentration always showing a larger value. While the estimates from depolymerization fraction and the overlap experiments are consistent, the dark regions in TEM are significantly smaller, indicating that this reaction pathway either requires higher temperature or multiple factors (such as confinement and temperature). The grey region indicates the predicted range from a phenomenological model which assumes that the local temperature falls off as 1/*r* moving away from the particle.

the overlap (starch luminescence, circle symbols) and depolymerization (square symbols) analysis results are consistent with each other, which indicates that the temperature profile is likely quite steep over the temperature range of *ca.* 120–185 °C, which should be sampled by these experiments. The discrepancy in the size of the degradation by-product regions is discussed in section 2.6 and indicates that the by-product formation requires additional factors aside from temperature. For a point-like source, the simplest model for the temperature distribution is $T(r) = \frac{AI}{r} + B$, where B is the background temperature far from each particle due both to the surroundings and the photothermal contribution to the global heating, r is the distance from the center of the particle, and A is a constant (providing that the particle extinction coefficient and heat loss from the surface are relatively constant). To determine if the depolymerization and overlap data in Fig. 12 are consistent with such a model, we set the temperature of the hot zone at either 140 or 185 °C and the average temperature equal to B (which is reasonable estimate for low concentrations[16]) and fit to determine A. Using a single value of A for all cases, the model predictions are shown as the gray background shape in Fig. 11, and are completely consistent with the data. This indicates that a $1/r$-like local temperature distribution is likely present.

3. Conclusions

In this work we have summarized and extended knowledge of the degradation process within polyethylcyanoacrylate (PECA) including depolymerization to monomer, a significant fraction of which repolymerizes to a daughter oligomer due inability to diffuse out of the sample. A luminescent degradation side product is observed, along with the insight that starch also becomes luminescent when warmed above 140 °C. These characteristics make PECA a useful material for studying (i) the relationship between mechanical properties and chemical degradation, and (ii) the ability of photothermal heating utilizing nano-objects to produce heterogeneous patterns of temperature. In particular, when exposed to photothermal heating using AgNPs, degradation occur dominantly in the warmest regions in the sample (*i.e.*, in the volumes immediately surrounding each nano-heater). This deterioration creates defect sites, the size of which can be controlled *via* the intensity of light utilized for photothermal heating, and number of which is directly related to the AgNPs concentration. These defect sites are correlated with decrease in tensile strength and thus, this nanoscopic property is quantitatively reflected in a macroscopic measurement. As a result, mechanical properties can be manipulated *via* a heterogeneous degradation process. Carbonaceous material formed as a side-product of the degradation process is also localized in the warmest regions and photothermal heating may be a pathway to the formation of graphene-like meso-structures at modest average temperatures. Through these relatively unusual properties, PECA is useful system to demonstrate the heterogeneous temperature field present during photothermal heating. Incorporation of starch particles in any polymeric system subjected to photothermal heating may be an additional useful strategy to confirm the non-uniform temperature distribution resulting from nanoparticle-based heating approaches.

4. Experimental methods

4.1. Polymerization

PECA was prepared by mixing ECA monomer (K&R international, *E–Z* bond 5 cP viscosity, 99% ECA) with an initiating agent (9 : 1 by volume of acetone (Fisher Chemical reagent grade, ≥99.5%) to deionized water (DI, Millipore, 18 MΩ) at room temperature. Acetone is a solvent for both ECA and PECA and enables homogeneous mixing of water and ECA. The OH– ions present within the water initiate the polymerization reaction.[23,26] PECA polymerization is an exothermic process. Our own research confirmed previous reports[20,27] indicating that pure PECA is brittle and exhibits poor mechanical strength. Addition of a small fraction of starch (Sigma-Aldrich, analytical grade starch derived from corn) to the polymer matrix, creating a composite in ratio 98 : 2 PECA : starch by weight (wt%), resulted in robust mechanical performance. The use of the lowest starch fraction possible ensured that the samples were highly transparent to visible light and simplified the analysis of mechanical degradation results. It is likely that traces of water on the starch powder also participate in the PECA polymerization.[23] Previous reports have fabricated PECA : starch composites having significantly higher starch content[23] (50–64 wt%). In our studies, reducing the starch content from 40 to 2 wt% decreased the Young's modulus and breaking strength by about 30% with no change in the strain at break. Thus, both low-starch and high-starch content PECA composites have good mechanical properties; additional starch content stiffens the composite material.

The typical fabrication procedure had polymerization occurring at room temperature in a laboratory environment with a relative humidity of 65%. 2 ml water/acetone mixture was added into 4 g ECA dropwise (at ~30 μL per drop) over 30 seconds with simultaneous magnetic stirring at ~1000 rpm. The ECA slowly polymerizes during this time as the acetone and water vapor gradually evaporate. After about 4 minutes, 0.1 g starch was added to the solution and stirring continued for another 2 minutes. The mixture was poured into an open-top plastic mold. PECA : starch composite films with an average thickness of 0.5 mm were removed from the mold after one hour and cut into rectangular shapes (8 mm × 100 mm). The resulting film samples were then placed into a 65 °C oven for 18 hours to ensure that the polymerization was complete and the acetone and residual water were fully evaporated. Without this final baking step, it was observed that samples stored at room temperature demonstrated changes in mechanical response over the following ~3 days before the maximum tensile properties were obtained, likely reflecting

incomplete polymerization under those circumstances. In contrast, the oven post-treated samples demonstrated the same maximum tensile properties immediately after the baking step with no further changes in mechanical properties occurring with time when stored at room temperature.

4.2. Synthesis and characterization of silver nanoparticles

AgNPs were synthesized using the Turkevich method:[41,42] 100 mL of aqueous solution containing 1 mM silver nitrate ($AgNO_3$, 1.7% (w/v) water solution, 17 g L^{-1}, RICCA chemical) was held in a closed-cap bottle, which was then placed in a heated water bath. When the bath began boiling, 10 mM of sodium citrate tribasic dihydrate (≥99%, Sigma-Aldrich), a reducing agent, was added and mixed well by shaking the bottle. The closed cap bottle was returned to the boiling water bath for one hour; the solution typically became bright yellow after ~30 min and an additional 30 min were utilized to ensure that the reaction and nanoparticle growth were complete. After cooling to room temperature, 100 mg polyvinylpyrrolidone (PVP, 360 kg mol^{-1}, Scientific Polymer Products, Inc.) was added as an additional capping and stabilization agent. Previous reports[43–47] indicate that PVP can ligand exchange[48] most of the sodium citrate on a metal nanoparticle surface.[49] The solution was then twice centrifuged (Eppendorf 5415 D) to facilitate removal of residual citrate and PVP, and to increase the AgNPs concentration. Note: addition of citrate-stabilized particles without PVP to ECA resulted in uncontrolled polymerization, in contrast, the PVP-coated particles had no discernible effect on ECA polymerization.

Ultraviolet–visible absorption spectroscopy (Cary 50) and transmission electron microscopy (TEM, JEOL 2000FX) were used to characterize the resultant AgNPs. Citrate-stabilized AgNPs in DI water had a primary peak at 420 nm (Fig. 13(a), solid line), consistent with a dominant particle size of 50 nm with a negligible oxide shell.[50] The 120 nm peak width (full-width-at-half-maximum, FWHM) of the observed localized surface plasmon resonance (LSPR) however indicates that the particles are not monodisperse. In particular, utilizing Mie theory, if particle size ranged from 40 to 60 nm in a uniform distribution the expected FWHM would be 130 nm, which is consistent with (though an over-estimate) the observed value. For TEM, AgNPs were concentrated *via* centrifugation and drop-cast on TEM grids. Size analysis from TEM images (*e.g.*, Fig. 13(b) inset) confirmed an average size of 50 ± 10 nm (N = 200) for silver spheroids. AgNPs formed *via* this method also contain some fraction of nanorods, which was less than 5% by number.

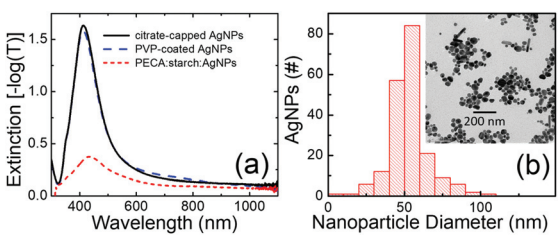

Fig. 13 (a) Extinction spectra of citrate-capped AgNPs in DI water (black solid line), re-suspended centrifuged PVP-coated AgNPs in DI water (blue dashed line), and 0.5 mm thick PECA : starch : AgNPs sample (red short dashed line). In each case, an appropriate background spectrum has been removed. (b) Histogram of AgNP spheroidal size distribution (all particles with an aspect ratio <2) resulting in an average size of 50 ± 10 nm. Inset: TEM image of citrate-capped AgNPs drop-cast from water.

In order to obtain the desired AgNPs concentration in the PECA composite, the AgNPs aqueous solution was concentrated by centrifugation to ~16× its original value. Tubes of 1 ml volume were centrifuged at 13.4 kRCF for 10 minutes and then re-suspended by adding 0.5 ml of 0.5 M PVP in water. This solution was centrifuged again and then re-diluted by adding 0.125 ml of 0.5 M PVP in water. Extinction spectroscopy after re-diluting the final solution with aqueous PVP solution to its original concentration (Fig. 13(a), blue dashed line) and of the final PECA samples (Fig. 13(a), red dotted line) indicated minimal change in extinction as a result of PVP-substitution, centrifugation, or incorporation within the samples. The primary peak for the re-diluted PVP–AgNPs solution occurs at 419 nm with a FWHM of 120 nm, nearly identical to the original solution. The observed peak in PECA : starch, occurs at 439 nm (FWHM of 140 nm), which matches the expected peak location (~450 nm) due to the change in dielectric constant (refractive index) of the surroundings from water to PECA. The peak width increases with refractive constant, with a predicted value of (assuming uniform distribution) of 155 nm, which is consistent with that observed experimentally.

PECA : starch : AgNPs samples were fabricated as described above apart by utilizing the AgNPs aqueous solution instead of water within the initiator agent. Based on the absorption-spectroscopy peak height of the resulting PECA : starch : AgNPs samples (Fig. 13(a), red dotted line) and the expected value of the extinction coefficient[51] of 50 nm AgNPs (5.37×10^{10} M^{-1} cm^{-1}), the final concentration of AgNPs at the highest loading level in the polymer composite was 0.003 wt%, which compares well with the ideal value of 0.004 wt% predicted from the measured concentration of the original solution.

Cross-sectional TEM image analysis was utilized to confirm that nanoparticles were present within micro-tomed PECA : starch : AgNPs samples and to determine the degree of dispersion and effective concentration. AgNPs were identified using 30 low magnification images (comprising a volume of 8 μm × 8 μm × 0.1 μm) to determine an operational photothermal object (nanoparticle or cluster) molarity (35 and 250 pM, respectively) for the two different AgNPs loadings. These values for the effective concentration are within a factor of 2 of the expected concentration given theoretically perfect dispersion of mono-sized AgNPs. For both concentrations, approximately 50% of the observed particles were isolated with the remaining 50% residing in aggregates. Only 2-particle aggregates were observed at the lower concentration; for 250 pM about 40% of the aggregates had 4 or 5 particles, with the remainder in particle pairs.

The effective concentrations given above were determined as follows. Even with the large TEM field size (8 μm × 8 μm),

for the lowest concentration the expected average value of less than 1 nanoparticle per field leads to a selection bias. In particular, the lack of a distinct object on which to optimize the image focus in regions of the film without AgNPs leads to underrepresentation. For the lower concentration, the raw molarity (*e.g.*, the number of observed particles either isolated or in clusters divided by the observed volume) was within a factor of 3 of the expected value. For the higher concentration (*i.e.*, 7× the lower concentration), the observed raw molarity (380 pM) was consistent with the expected value of 400 pM. After these checks, the effective concentration was determined by starting from the amount of AgNPs material incorporated in the sample and accounting for the effect of clustering (*e.g.*, if 50% of the particles are in pairs, then the effective concentration of objects is ~75% of the intended value).

4.3. Degradation protocols

4.3.1. Conventional heat treatment protocol. PECA : starch and PECA : starch : AgNPs samples were conventionally heated to study their thermal stability and enable comparison with photothermally-heated PECA : starch : AgNPs samples. Nanocomposite film samples were placed in an oven at a preselected temperature (between 20 °C and 215 °C) for 1 hour.

4.3.2. Photothermal heat treatment protocol. PECA : starch : AgNPs specimens underwent laser illumination having a wavelength of 445 nm at selected fixed intensity values ranging from 0.3 W cm^{-2} to 1 W cm^{-2} for 1 hour. The laser wavelength was selected to excite the LSPR of the embedded silver nanoparticles. A 1.5 W laser beam (home built, continuous-wave system, consisting of 1.8 W A-Type M140 diode mounted in a 12 mm × 30 mm copper module and a fan-cooled heat sink, powered by an external current-controlled driver) was expanded through a cylindrical lens and spatially-overlapped with a similarly-constructed 1 W laser so that the combined beams illuminated a rectangular area (~1 cm × 3 cm) where film samples were mounted. Average light intensity could be varied by adjusting a non-polarizing plate beam splitter in the beam path. The combined heating beams were amplitude-modulated at 6 Hz with an 85% duty cycle (see timing diagram in ESI Fig. S4†) to enable a brief interruption of the 445 nm irradiation to facilitate an optical thermometry measurement for determination of average sample temperature (see section 4.6). PECA : starch composite samples (*e.g.*, Ag-free) exposed at the highest intensity for 1 hour confirmed that any non-specific heat generated was at a low level compared to the photothermally-driven process and did not degrade the PECA : starch samples.

4.4. Characterization of mechanical properties, molecular weight, and mass loss

Tensile testing was utilized to characterize mechanical properties of composite samples during the degradation process. Specimens of PECA : starch and PECA : starch : AgNPs composites were fabricated as rectangular films (100 mm long × 8 mm wide × 0.5 mm thick), which were measured in their untreated as-made condition or after specific thermal exposure from conventional or photothermal heating. For each heat treatment condition, 10 specimens or more were subjected to mechanical testing. Note that for photothermal heating, the laser illumination area fully encompassed the entire gauge length (30 mm × 8 mm) of the sample. A single column tabletop testing system (Instron 5944) equipped with a 2 kN load cell and Bluehill 3 software for data recording and analysis was utilized. All mechanical tests were conducted at room temperature with a relative humidity of 65% and an extension rate of 0.5 mm min^{-1}. The gauge length was fixed at 30 mm to match the ASTM-D695 standard regarding sample length to width ratio. Paper frames were used to prevent grip point failure.

Thermal stability of the PECA : starch composite was quantified by thermogravimetric analysis (TGA, PerkinElmer Pyris 1). For the data shown in Fig. 1, samples were heated in a platinum sample holder under nitrogen gas (dashed blue line) or air (solid black line) at a heating rate of 10 °C min^{-1} from 20 to 400 °C. Significant mass loss begins at ~175 °C (180 °C) and maximum degradation occurs at 265 °C (270 °C) in air (nitrogen), respectively. Although degradation occurs at slightly lower temperatures in air, there is no dramatic effect due to the presence of oxygen, which is expected given the current understanding of the depolymerization reaction (see section 2.2), which is thermally-activated and oxygen-independent. The polymer was completely degraded at 290 °C in both cases, consistent with previous reports.[20–22] A single degradation feature due to the PECA is observed because the deterioration of starch (which is observed at 310 °C in PECA : starch composites with a higher wt% starch content) is highly-suppressed due to the minute amount present (2 wt%).

Molecular weight measurements of PECA *via* gel permeation chromatography (GPC) utilized a Waters HPLC with Alliance 2696 pump and 2414 RI detector having a flow rate of 1.25 μL min^{-1}. Molecular weight was calibrated with Agilent EasiCal GPC Polystyrene standards A & B. Each standard spatula contained 5 polymer weights to calibrate a range from 580 to 6 870 000 Daltons. PECA : starch samples as-fabricated and having undergone conventional heat treatments (at several temperatures) were dissolved in tetrahydrofuran (THF) at a concentration of 10 mg ml^{-1}. Starch was filtered from the solution prior to measurement. Number-average M_n and weight-average M_w molecular weight were calculated to determine how molecular weight distribution changed under conventional thermal degradation.

GPC studies of PECA can potentially be complicated by solution-driven degradation and repolymerization of ECA to form oligomers.[21,52,53] To test if such a process was present, solutions of as-made PECA composite samples were prepared, allowed to remain in solution for 1–5 days, and subjected to GPC (Fig. 14). In all cases, the data showed no trends with time in solution, indicating that a solution degradation process is not present. Data from multiple batches of as-made samples and data from samples exposed to different holding times in solution all consistently resulted in a number averaged molecular weight of 50 000 ± 7800 g mol^{-1}. Thermally-degraded samples had distinctively different retention times

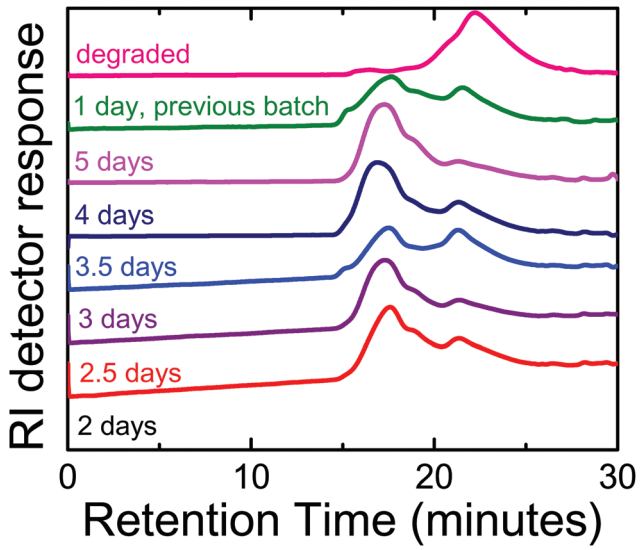

Fig. 14 GPC measurements of intensity *versus* retention time for as-made PECA : starch composite samples (lower 6 curves shown) measured between 2–5 days after solvation in THF. The second curve down from the top shows data from a separate batch of samples, measured 1 day after solution preparation. All as-made data is self-consistent, indicating no evidence of a solution degradation process. The top curve demonstrates the observed changes in retention time due to thermal degradation at 215 °C for 1 hour (see also Fig. 2(b)).

(top curve in Fig. 14), corresponding to a molecular weight decrease by an order of magnitude.

The average molecular weight of photothermal-heated PECA : starch : AgNPs samples were measured at 20 °C *via* calibrated dilute solution viscometry (Cannon, Ubbelohde 9721-R53), as the presence of metal nanoparticles prevented use of GPC due to concerns of instrument contamination. Mark–Houwink coefficients to determine number-averaged molecular weight for PECA in THF in the pertinent M_n range have been previously reported.[54] These coefficients were confirmed by dilute solution viscometry measurements on as-made and conventionally-degraded (at 100 °C, 120 °C, 150 °C, 170 °C, 180 °C, 185 °C, and 190 °C) PECA : starch samples with known molecular weight from GPC at 3–4 different concentrations per sample type. Solutions were filtered to eliminate starch before measurement. Extrapolating $\ln\left(\frac{t}{t_0}\right)/c$ to zero concentration, where t is transfer time, t_0 transfer time for the solvent only, and c the concentration in mg ml^{-1} provided the most reliable prediction of M_n. Control experiments enabled determination of K'' values where $\eta(c) = [\eta] + [\eta]^2 K''c$, and those K'' values were used to find $[\eta]$ from PECA : starch : AgNPs solution measurements at a concentration of 10 mg ml^{-1}, selected because measurements were the most reliable at this concentration.

4.5. Characterization of morphology and observation of degradation-related polymer luminescence

As-made and degraded sample morphologies were analyzed *via* scanning electron microscopy (SEM, Hitachi S-3200N). AgNPs placement and sample morphology were also quantified *via* TEM on micro-tomed (Leica UC7 Cryo Ultramicrotome) slices of ~100 nm thickness.

Bright field microscopy (Nikon Eclipse 90i) images were taken to explore surface and near surface morphology on larger size scales. For some samples, the low content starch filler was exposed to iodine dye before incorporation in the PECA sample in order to improve contrast under the bright field imaging. 5–10 grams of starch was placed in a glass beaker and mixed with ~30 ml of 10% aqueous iodopovidone (Purdue Products L.P.) to create a slurry. After 1 hour in the closed vessel, pressure-assisted filtration was utilized to collect the dyed starch, which was repeatedly, copiously rinsed in de-ionized water and filtered with pressure-assistance until the filtrate was clear. Starch was dried overnight at room temperature before use. Fluorescence microscopy measurements to observe degraded starch and PECA were performed utilizing a DAPI-5060 filter set to provide the excitation spectral pathway (350 to 400 nm) coupled with an emission filter pass band (450 to 500 nm).

Development of optical absorption and luminescence from degraded polymers and biopolymers is a relatively common phenomenon. Recent work has summarized existing literature and reported data from a range of chemically-different polymeric materials that all develop a similar, characteristic luminescence upon degradation.[36,55,56] The prototypical emission has an unstructured broad absorption and emission curves, significant overlap between excitation and emission wavelength ranges, and is highly-depolarized (particularly at higher emission wavelengths), indicating that the luminescence results from a many-step energy migration process through interacting electronic states. Here we report observing similar emission from both pure PECA and starch samples after exposure to elevated temperatures.

Emission curves from as-made and degraded samples were collected (Photon Technology International, Quanta Master 40). A linearly polarized excitation source was created *via* a Xenon lamp source filtered through a monochromator set at 403 nm with 3 nm slits, followed by a 10 nm bandpass filter centered at 405 nm and a Glan-Thompson polarizer in the excitation pathway. Spectrally-resolved luminescence in the range 415–725 nm was detected by a photomultiplier tube filtered by a second polarizer set at the magic angle of 54.7° through a detection path monochromator with 1 nm slits, using a 1 nm step size and a 2 s per step integration time. By rotating the Glan-Thompson filters, fluorescence anisotropy curves for the emission can also be calculated, as $r = \frac{I_{\parallel} - GI_{\perp}}{I_{\parallel} + 2GI_{\perp}}$ where G calibrates the detector's polarization response and $I_{\parallel}$ ($I_{\perp}$) is the emission detected parallel (perpendicular) to the excitation polarization direction.

As demonstrated in Fig. 15, PECA, conventionally degraded by being held at 182 °C for 0.75 hours, was found to have a broad emission centered at ~490 nm when excited in the range 350 to 400 nm (red dashed curve, excited at 403 nm). As

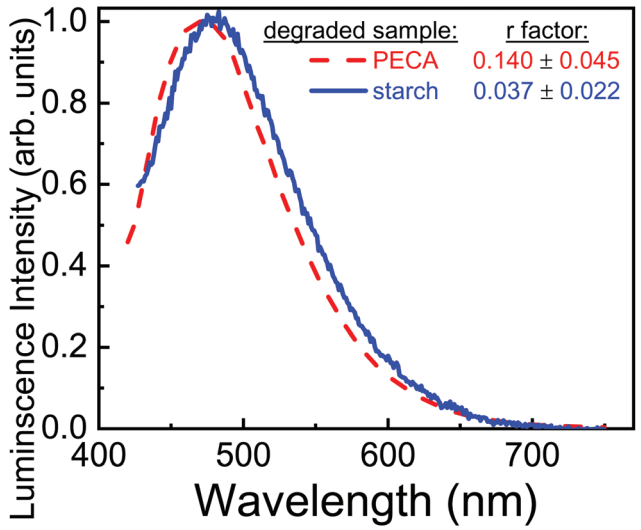

Fig. 15 Spectrally-resolved luminescence curves from pure PECA and pure starch samples, after thermal degradation using conventional heating. Anisotropy measurements reveal the emission is highly-depolarized, consistent with a previous report[36] from different polymeric systems.

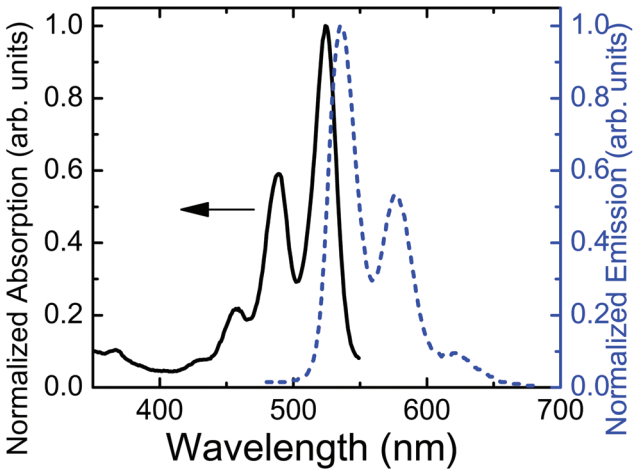

Fig. 16 Absorption (left axis) and emission (right axis) spectra of an as-made PECA : starch film sample with incorporated Lumogen Orange at room temperature. To enable observation of the full emission spectrum, an excitation wavelength of 445 nm was utilized here.

well, pure starch samples which were degraded by conventional thermal treatment at 200 °C for 1 hour (Fig. 15, blue solid curve) also displayed a similarly wide and featureless emission peak. (The degraded starch emission curve is scaled to the peak of the degraded PECA emission for ease of comparison.) In contrast, as-made PECA : starch film samples displayed no such emission (see ESI Fig. S5†). The degree of depolarization of the emission can be quantified from the r factor, where values range from 0.4 (indicating maximum correlation between excitation and emission polarization directions, as would be expected for a simple fixed fluorophore) to 0 (complete depolarization) as the correlation between the input and output polarization direction decreases, assuming ideal parallel absorption and emission dipoles. We observe over the range 450–650 nm that $r = 0.037 \pm 0.022$ for starch and $r = 0.14 \pm 0.045$ from PECA after thermal treatments. Both the similarity of the emission curves to each other and their similarity to that previously reported argue that starch and PECA exhibit degradation-related luminescence.

4.6. Molecular fluorescence thermometry

The average temperature within the highly-transparent sample was monitored *via* fluorescence from embedded fluorophores. Lumogen Orange F 240 (BASF) is a perylene-derivative molecule which absorbs in the range of 425–550 nm (Fig. 16, black curve, left axis), thus enabling the use of 532 nm light to preferentially excite the fluorophores rather than the AgNPs in the sample (compare with Fig. 13(a)). Use of excitation source at 532 nm also avoided creation of any parasitic luminescence from degraded starch and PECA (see section 4.5), which would provide contaminating signals for the non-contact fluorescence thermometry measurement. However, though selected against, the strong 445 nm laser used to drive the photothermal heating of the AgNPs will also excite the Lumogen Orange: to avoid detector saturation from this signal, a gating scheme was employed by briefly interrupting the heating laser to make the temperature measurement (see ESI Fig. S4†).

A low concentration solution of Lumogen Orange in acetone was introduced into the PECA : starch : AgNPs system during polymerization initiation to result in a mass fraction of 0.0005 wt% in the final solid sample. A low-power 532 nm laser (5 mW), collimated to 0.3 cm diameter and amplitude-modulated at 1 kHz, was used as an excitation source. Fluorescence from the excited spot was imaged onto a spectrometer (SPEX 1680B), whose output was measured with a photomultiplier tube (PMT, Hamamatsu 931B). Cut off filters (Thorlabs FGL 455, Newport 10CGA-475) were utilized to reject scattered 445 nm heating beam laser light. The PMT output signal was passed into a lock-in amplifier (Stanford Research Systems, SR830) referenced to the 1 kHz modulation, and the measurement triggered by a brief interruption of the 445 nm heating laser. In summary, both the intense 445 nm heating beam and the weak 532 nm thermometry illumination will excite the Lumogen Orange and result in fluorescence. By momentarily (6 Hz; 85% duty cycle) turning off the 445 nm beam and then syncing a fluorescence measurement selectively using the 1 kHz modulation of the 532 nm beam, a sensitive measurement of emission (and thus temperature) can be obtained without saturating the detector, and independent of the 445 nm heating beam intensity.

Calibration for the molecular fluorescence thermometry was accomplished by conventionally heating a sample clamped to a copper block attached to a hot plate to various specified temperatures. Examples of spectrally-resolved fluorescence curves for 8 different temperatures between 20–185 °C appear in Fig. 17(a). As with neat perylene,[15,16,57–63] with judicious choice of two distinct wavelengths within the

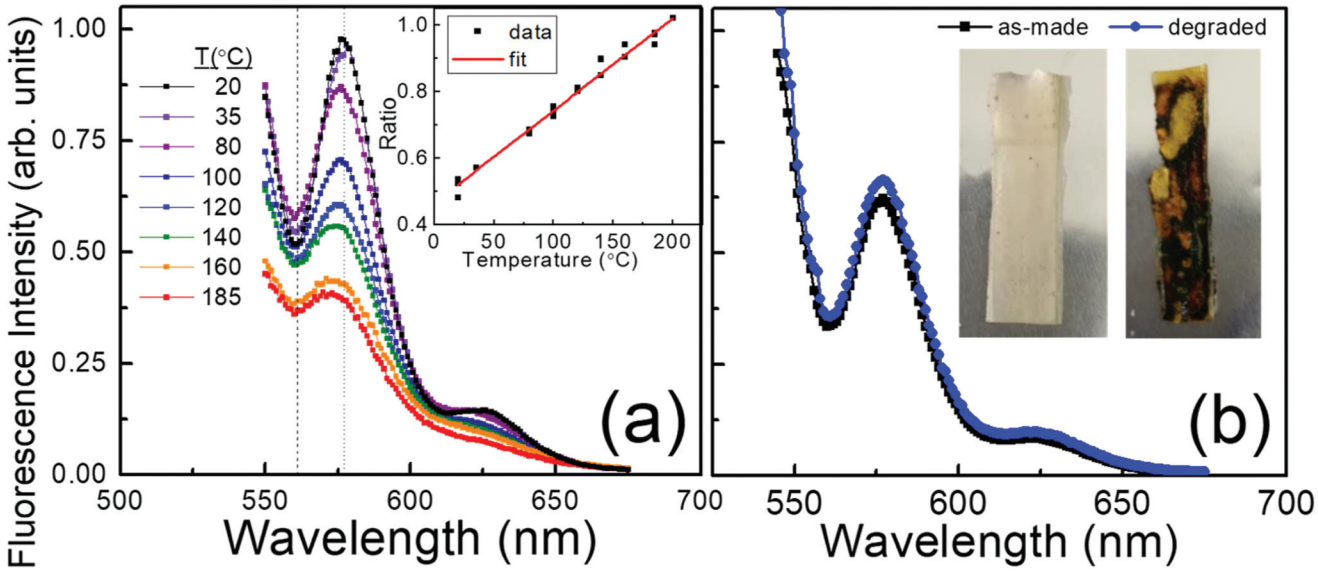

Fig. 17 (a) Spectrally-resolved Lumogen Orange emission spectra *versus* temperature under conventional heating of composite film samples. The vertical dashed and dotted lines indicate the location of the two wavelengths chosen for the ratio calculation. Inset: Emission intensity ratio from fluorescence at 561 nm to that at 577 nm has a linear relation to sample temperature. (b) Lumogen Orange emission spectra (excited at 532 nm) measured at 20 °C as-made (black data) and after thermal degradation (blue data) by conventional heating at 185 °C for one hour display identical shape and structures. The overall fluorescence amplitude decreases and the data presented has been normalized. Inset: Optical images of the sample before and after degradation.

emission spectrum (ranging from 510–625 nm, Fig. 16, blue curve, right axis, but accessible from 533–625 nm here) a measured ratio of emission signals can be found which is proportional to the sample temperature. In particular, for Lumogen Orange, the ratio of the emission intensity at the "trough" at 561 nm to that of the "peak" at 577 nm increases linearly as a function of temperature (Fig. 17(a) inset).

PECA starts to degrade when a sample temperature of 150 °C is reached or exceeded, and changes occur quite rapidly at 185 °C. When being excited at 532 nm during this process, the Lumogen Orange emission overall decreased as the sample becomes less transparent, but the selected ratio measurement showed no changes with ongoing polymer degradation, indicating that the fluorescence thermometry approach is robust to the underlying deterioration of the polymer. Fig. 17(b) compares the Lumogen Orange emission spectra before and after a sample is conventionally heated to 185 °C for one hour. During the heat treatment, the specimen experiences a 20% mass loss and a complete loss of mechanical stability, indicating significant degradation (see inset to Fig. 17(b) for before and after sample optical images). The spectra before and after degradation have an identical shape and the resultant room-temperature ratios match within error. During heating, the ratio remains constant throughout the degradation process (data not shown), correctly reflecting that the sample is held at 185 °C.

Conflicts of interest

There are no conflicts to declare.

Acknowledgements

This research was supported by the National Science Foundation (grants CMMI-0829379, CMMI-1069108, and CMMI-1462966). This work was performed in part at the Analytical Instrumentation Facility (AIF) at North Carolina State University, which is supported by the State of North Carolina and the National Science Foundation (grant ECCS-1542015). The AIF is a member of the North Carolina Research Triangle Nanotechnology Network (RTNN), a site in the National Nanotechnology Coordinated Infrastructure (NNCI). Some work was also performed in the NC State Physics Education and Research Laboratory (EaRL). The authors thank Prof. Keith Weninger, Prof. Jan Genzer, and Prof. Stephen Michielsen for use of equipment, and Prof. Wendy E. Krause for useful discussions. Additionally, we gratefully acknowledge Ms Birgit Anderson for helping with DSC, TGA, GPC measurements, Mr Yeongun Ko for helping with GPC analysis, and Mr Toby Tung for helping with the TEM imaging.

References

1 B. C. Daglen and D. R. Tyler, *Green Chem. Lett. Rev.*, 2010, **3**, 69–82.
2 E. Eastwood, S. Viswanathan, C. P. O'Brien, D. Kumar and M. D. Dadmun, *Polymer*, 2005, **46**, 3957–3970.
3 R. W. Cahn, P. Haasen and E. J. Kramer, *Phase transformations in materials*, VCH, Weinheim, 1991.

4 Y. Toi and S.-S. Kang, *Trans. Jpn. Soc. Mech. Eng., Ser. A*, 2004, **70**, 9–16.
5 R. C. Thompson, C. J. Moore, F. S. vom Saal and S. H. Swan, *Philos. Trans. R. Soc., B*, 2009, **364**, 2153–2166.
6 J. Hammer, M. H. S. Kraak and J. R. Parsons, *Reviews of Environmental Contamination and Toxicology*, Springer, New York, 2012, vol. 220, pp. 1–44.
7 G. Firestone, H. Huang, J. R. Bochinski and L. Clarke, *Nanotechnology*, 2019, **30**, 475706.
8 M. Eriksen, L. C. M. Lebreton, H. S. Carson, M. Thiel, C. J. Moore, J. C. Borerro, F. Galgani, P. G. Ryan and J. Reisser, *PLoS One*, 2014, **9**, 15.
9 P. K. Jain, X. Huang, I. H. El-Sayed and M. A. El-Sayad, *Plasmonics*, 2007, **2**, 107–118.
10 P. K. Jain, X. Huang, I. H. El-Sayed and M. A. El-Sayed, *Acc. Chem. Res.*, 2008, **41**, 1578–1586.
11 K. L. Kelly, E. Coronado, L. L. Zhao and G. C. Schatz, *J. Phys. Chem. B*, 2003, **107**, 668–677.
12 D. Jaque, L. M. Maestro, B. del Rosal, P. Haro-Gonzalez, A. Benayas, J. L. Plaza, E. M. Rodriguez and J. G. Sole, *Nanoscale*, 2014, **6**, 9494–9530.
13 X. H. Huang, P. K. Jain, I. H. El-Sayed and M. A. El-Sayed, *Lasers Med. Sci.*, 2008, **23**, 217–228.
14 Z. Qin and J. C. Bischof, *Chem. Soc. Rev.*, 2012, **41**, 1191–1217.
15 S. Maity, W. C. Wu, C. Xu, J. B. Tracy, K. Gundogdu, J. R. Bochinski and L. I. Clarke, *Nanoscale*, 2014, **6**, 15236–15247.
16 S. Maity, W.-C. Wu, J. B. Tracy, L. I. Clarke and J. R. Bochinski, *Nanoscale*, 2017, **9**, 11605–11618.
17 K. Vanherck, S. Hermans, T. Verbiest and I. Vankelecom, *J. Mater. Chem.*, 2011, **21**, 6079–6087.
18 S. Maity, L. N. Downen, J. R. Bochinski and L. I. Clarke, *Polymer*, 2011, **52**, 1674–1685.
19 C. Birkinshaw and D. C. Pepper, *Polym. Degrad. Stab.*, 1986, **16**, 241–259.
20 M. G. Han, S. Kim and S. X. Liu, *Polym. Degrad. Stab.*, 2008, **93**, 1243–1251.
21 F. Leonard, J. A. Collins and H. J. Porter, *J. Appl. Polym. Sci.*, 1966, **10**, 1617–1623.
22 K. G. Chorbadjiev and P. C. Novakov, *Eur. Polym. J.*, 1991, **27**, 1009–1015.
23 S. Kim and S. C. Peterson, *Polym. Compos.*, 2012, **33**, 904–911.
24 E. Kung, A. J. Lesser and T. J. McCarthy, *Macromolecules*, 2000, **33**, 8192–8199.
25 H. Ablat, I. Povey, R. O'Kane, S. Cahill and S. D. Elliott, *Polym. Chem.*, 2016, **7**, 3236–3243.
26 C. Loschen, N. Otte and E. Radchenko, *Macromolecules*, 2010, **43**, 9674–9681.
27 I. Skeist, *Handbook of adhesives*, Van Nostrand Reinhold, New York, 3rd edn, 1990.
28 A. Hickey, J. J. Leahy and C. Birkinshaw, *Macromol. Rapid Commun.*, 2001, **22**, 1158–1162.
29 J. M. Rooney, *Br. Polym. J.*, 1981, **13**, 160–163.
30 CROW, *Chemical Retrieval on the Web (CROW)*, 2019, https://polymerdatabase.com/.
31 T. A. Bykova, Y. G. Kiparisova, B. V. Lebedev, K. A. Mager and Y. G. Gololobov, *Polym. Sci. U.S.S.R.*, 1991, **33**, 537–543.
32 A. A. Griffith and G. I. Taylor, *Philos. Trans. R. Soc., A*, 1921, **221**, 163–198.
33 E. Mele, J. A. Heredia-Guerrero, I. S. Bayer, G. Ciofani, G. G. Genchi, L. Ceseracciu, A. Davis, E. L. Papadopoulou, M. J. Barthel, L. Marini, R. Ruffilli and A. Athanassiou, *Sci. Rep.*, 2015, **5**, 13.
34 T. Nahum, H. Dodiuk, S. Kenig, A. Panwar, C. Barry and J. Mead, *Nanotechnol., Sci. Appl.*, 2017, **10**, 53–68.
35 R. P. Wool, *Macromolecules*, 1993, **26**, 1564–1569.
36 R. Steffen, G. Wallner, J. Rekstad and B. Röder, *Polym. Degrad. Stab.*, 2016, **134**, 49–59.
37 D. Damodar, S. K. Kumar, S. K. Martha and A. S. Deshpande, *Dalton Trans.*, 2018, **47**, 12218–12227.
38 A. Torchi, F. Simonelli, R. Ferrando and G. Rossi, *ACS Nano*, 2017, **11**, 12553–12561.
39 R. Marasini, A. Pitchaimani, T. D. T. Nguyen, J. Comer and S. Aryal, *Nanoscale*, 2018, **10**, 13684–13693.
40 B. V. Parakhonskiy, W. J. Parak, D. Volodkin and A. G. Skirtach, *Langmuir*, 2019, **35**, 8574–8583.
41 J. Turkevich, P. C. Stevenson and J. Hillier, *Discuss. Faraday Soc.*, 1951, 55–75.
42 Z. S. Pillai and P. V. Kamat, *J. Phys. Chem. B*, 2004, **108**, 945–951.
43 A. Rostek, D. Mahl and M. Epple, *J. Nanopart. Res.*, 2011, **13**, 4809–4814.
44 D. Mahl, C. Greulich, W. Meyer-Zaika, M. Koller and M. Epple, *J. Mater. Chem.*, 2010, **20**, 6176–6181.
45 K.-S. S. Chou and Y.-S. S. Lai, *Mater. Chem. Phys.*, 2004, **83**, 82–88.
46 H. H. Huang, X. P. Ni, G. L. Loy, C. H. Chew, K. L. Tan, F. C. Loh, J. F. Deng and G. Q. Xu, *Langmuir*, 1996, **12**, 909–912.
47 Y. G. Sun and Y. N. Xia, *Science*, 2002, **298**, 2176–2179.
48 S. Perumal, Ph.D. thesis, Freie Universität Berlin, Berlin, 2012.
49 S. Satapathy, J. Mohanta and S. Si, *ChemistrySelect*, 2016, **1**, 4940–4948.
50 D. Paramelle, A. Sadovoy, S. Gorelik, P. Free, J. Hobley and D. G. Fernig, *Analyst*, 2014, **139**, 4855–4861.
51 J. R. G. Navarro and M. H. V. Werts, *Analyst*, 2013, **138**, 583–592.
52 D. R. Robello, T. D. Eldridge and M. T. Swanson, *J. Polym. Sci., Part A: Polym. Chem.*, 1999, **37**, 4570–4581.
53 B. Ryan and G. McCann, *Macromol. Rapid Commun.*, 1996, **17**, 217–227.
54 E. F. Donnelly and D. C. Pepper, *Makromol. Chem., Rapid Commun.*, 1981, **2**, 439–442.
55 R. Steffen, M. Meir, J. Rekstad, B. Röder, B. Roder and B. Röder, *Polymer*, 2018, **136**, 71–83.
56 R. Steffen, H. Setyamukti, G. Wallner, K. Geretschläger, B. Röder, K. Geretschlaeger and B. Roeder, *Polym. Degrad. Stab.*, 2017, **140**, 114–125.
57 D. B. Abbott, S. Maity, M. T. Burkey, R. E. Gorga, J. R. Bochinski and L. I. Clarke, *Macromol. Chem. Phys.*, 2014, **215**, 2345–2356.

58 J. Dong, G. E. Firestone, J. R. Bochinski, L. I. Clarke and R. E. Gorga, *Nanotechnology*, 2017, **28**, 065601.
59 G. Firestone, J. R. Bochinski, J. S. Meth and L. I. Clarke, *J. Polym. Sci., Part B: Polym. Phys.*, 2018, **56**, 643–652.
60 S. Maity, J. R. Bochinski and L. I. Clarke, *Adv. Funct. Mater.*, 2012, **22**, 5259–5270.
61 S. Maity, K. A. Kozek, W. C. Wu, J. B. Tracy, J. R. Bochinski and L. I. Clarke, *Part. Part. Syst. Charact.*, 2013, **30**, 193–202.
62 V. Viswanath, S. Maity, J. R. Bochinski, L. I. Clarke and R. E. Gorga, *Macromolecules*, 2013, **46**, 8596–8607.
63 V. Viswanath, S. Maity, J. R. Bochinski, L. I. Clarke and R. E. Gorga, *Macromolecules*, 2016, **49**, 9484–9492.